1973

Some aspects of the phenomenon of superheating as exhibited by several fluids

John J. Morgan
Lehigh University

SOME ASPECTS OF THE PHENOMENON OF SUPERHEATING AS EXHIBITED BY SEVERAL FLUIDS

by

John J. Morgan

A Thesis

Presented to the Graduate Committee

of Lehigh University

in Candidacy for the Degree of

Master of Science

in

Mechanical Engineering

Lehigh University

1972

This thesis is accepted and approved in partial fulfillment of the requirements for the degree of Master of Science.

Nov. 22, 1972
(date)

John C. Chen
Professor in Charge

Ferdinand P. Beer
Chairman of Department

TABLE OF CONTENTS

LIST OF FIGURES

LIST OF TABLES

ABSTRACT

After a brief definition of the phenomenon of superheating, two distinct aspects are studied in detail. In the first a statistical method is devised to predict most probable superheat at inception as a function of temperature ramp which the fluid experiences. Data available from tests involving uniform steps of superheat are manipulated and combined to approximate the nature of a temperature ramp. An experimental program, while only of a simple form, yields strong qualitative support of the theory.

The probability distributions for inception for three particular ramps--2-3/4, 5, and 9-1/2°F/min--were experimentally determined, and the most probable superheat at inception taken from the distribution. To evaluate the theory three particular step tests--12, 22 and 32°F superheat--were run about 20 times each. These results were then used to synthesize probability distributions for the ramps of interest, and most probable superheats were again recorded. The qualitative comparison of the two sets of results shows good agreement: as ramp increases, the probability distribution peak decreases and most probable

superheat increases. Quantitatively, there is about a 25% maximum error due primarily to the grossness of the experiment.

The second section deals with determining the location of inception in a flowing superheated liquid. The assumption is that cavitation actually occurs in the low pressure centers of vortices shed by flow over obstructions. A free vortex model is used to demonstrate that a large pressure variation conducive to cavitation is found across a vortex. This variation increases with Reynolds number, thus stimulating cavitation or inception. This supports liquid potassium data from Brookhaven National Laboratory which indicates that superheat decreases as Reynolds number increases.

PREFACE

With ever increasing demands for electric power and only finite amounts of fossil fuel and hydro sources, nuclear power will be a necessity in the long run. But nuclear fuel reserves are not limitless, either. In order to obtain maximum utilization of nuclear fuel materials available, it will be necessary to develop breeder reactors--reactors whose fuels produce more fissile atoms than are consumed in the reactor.

The power density in a fast breeder reactor is very high. For this reason the coolant used must have excellent heat transfer properties. Liquid metals--sodium and potassium in particular--are ideally suited for this purpose and have become popular choices for fast breeder reactor coolants. One important characteristic of liquid metals is their ability to superheat, or maintain a temperature above the accepted saturation temperature for the given conditions. On a heat flux plot this tendency is noted as a deviation from the normal boiling curve. Figure A indicates how the superheat pattern differs from the normal pattern.

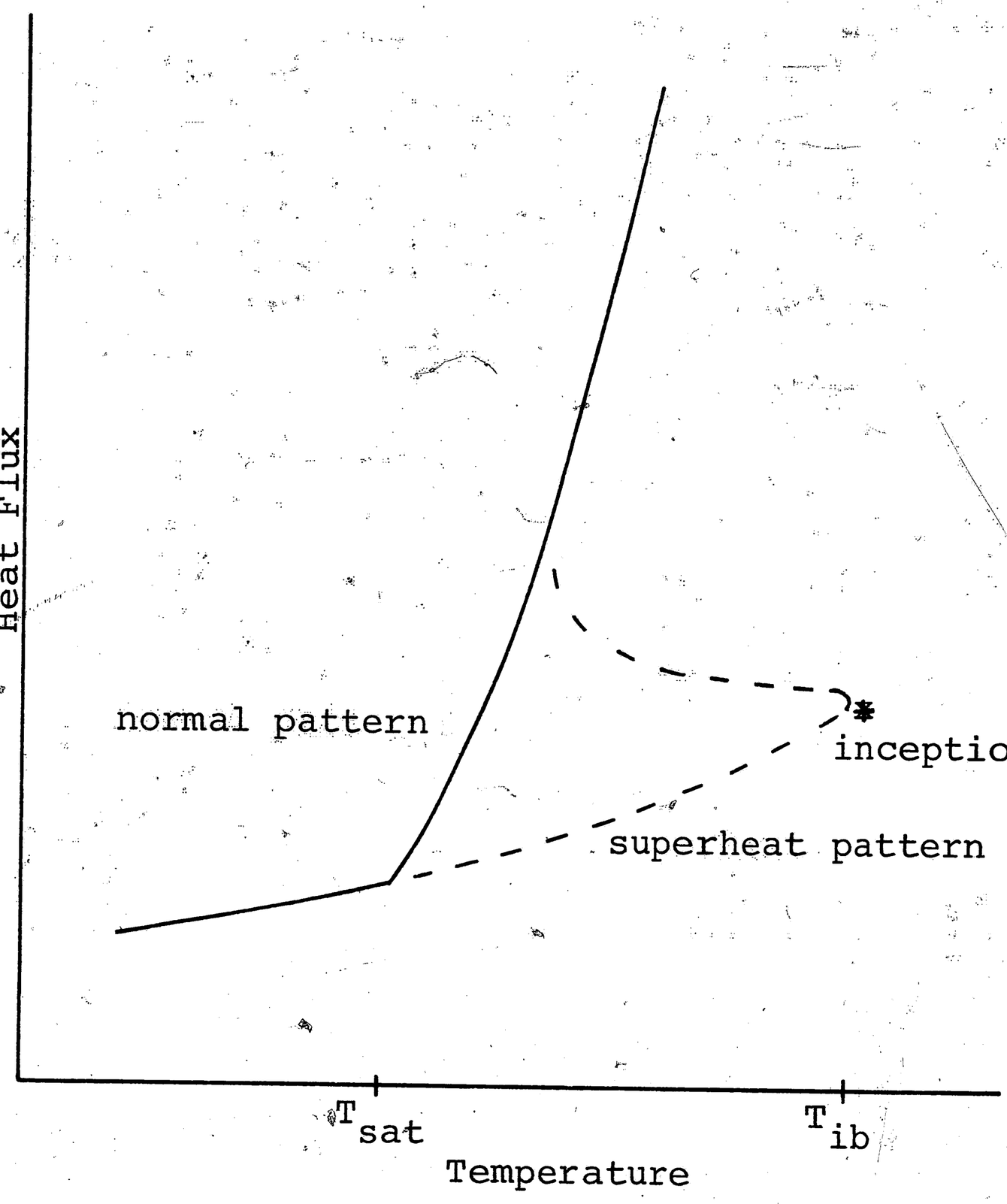

Figure A. Normal boiling curve and superheating pattern.

Due to the importance of liquid metal technology, studies have been conducted to investigate the causes of superheating, as well as methods to predict how much superheat will be sustained before inception and where in the system inception is likely to occur. This work is broken into two distinct parts dealing with separate aspects of the phenomenon. Part I uses the statistical nature of the problem to establish a theory of prediction based upon concepts of probability and relative frequency. Experimental results are included in support of this theoretical approach. Part II delves into inception location. In particular it involves a theoretical look at occurrence in the low-pressure cores of vortices shed as the flow crosses thermocouples, pressure taps, or other irregularities in the stream.

Although the two parts have been integrated for this thesis, it should be realized that they are separable and involve very different considerations. The pages, figures, and references have been numbered consecutively throughout, but symbols have been separated by part due to the quantity of same. It is the sincere hope of the author that this work will be followed by others of a more sophisticated and far-reaching nature.

J. J. M.
11/23/72

PART I

A STATISTICAL MODEL TO PREDICT MOST PROBABLE SUPERHEAT AT INCEPTION

INTRODUCTION TO PART I

The question of predicting the superheat at which inception occurs has never been adequately answered. Data available shows a scatter which is hard to reconcile. One theory attributes the superheat at inception to be solely a function of temperature ramp, or increase in temperature per unit time; and in fact this theory does appear to reduce the scatter significantly. However, the very nature and extent of the scatter found in experimental results have caused the author to look in a slightly different direction for the answer.

It is apparent that a great number of variables influence inception. These include properties of the specific fluid such as surface tension, viscosity, and heat transfer characteristics; the presence of impurities or dissolved gas in the liquid; the nature of the flow; temperature gradients involved; and the area and condition of the surfaces which provide sites for inception to occur.

Perhaps there are many more unrecognized variables as well. In any event it was the feeling of the author that a theory involving probability and statistics could best describe results being collected. This is not to say that inception in a superheated liquid is based on probability in nature; but that so many factors influence inception that a statistical nature appears.

With this thought the author proceeds to develop a rudimentary statistical theory which makes use of uniform temperature test results to predict results for tests of constant temperature ramp. While the results have been severely limited by the scope of the project, it is interesting to note that the theoretical predictions clearly indicate the qualitative nature of the experimental results. Also, there is reason to believe that if the experimental portion of this work was refined and expanded, the quantitative comparison would improve. However, it was the purpose at this time only to show that such a theory was a forward step in the prediction of attainable superheats.

STATISTICAL PREDICTION OF SUPERHEATS IN FLUIDS EXPERIENCING A CONSTANT TEMPERATURE RAMP

Probabilistic Terms and Laws

Before proceeding it is beneficial to list and define some of the mathematical terms and laws which will be used to develop the theory herein:

1) experiment - An experiment is any defined process, i.e., tossing a coin, rolling a die.

2) trial - A trial is the single carrying out of a specified experiment.

3) event - An event is the outcome of a single trial.

4) probability - Probability may be defined in terms of the likelihood of a specified event E; $\bar{E}$ indicates the failure of E to occur. Thus E and $\bar{E}$ are complementary and mutually exclusive events. As is conventional, p(E) signifies the probability of occurrence of E, and $p(\bar{E})$ the probability that E will not occur. Therefore, $p(E) + p(\bar{E}) = 1$.

5) relative frequency - Relative frequency theory is based on observational concepts. With m occurrences of event E in N trials of a specified experiment, the relative frequency of event E is defined as

$R(E) = m/N$. The relative frequency of $\bar{E}$ is given by $R(\bar{E}) = (N-m)/N$. Relative frequencies tend to stabilize as N increases. Assuming the existence of a limiting value, p(E) is defined as the limit of the relative frequency as the number of trials is increased infinitely. Therefore, $p(E) = \lim_{N\to\infty} R(E)$.

6) mutually exclusive events - Those events whose simultaneous occurrence is impossible are mutually exclusive.

7) independent events - Events are independent if the probability of the first given the second is equal to the probability of the first.

8) probability distribution or density function - The probability distribution function f(x) expresses the probability of the variate associated with any one of its admissible values. (See Figure 1a.)

9) cumulative distribution or probability function - The cumulative distribution function F(x) expresses the accumulated probability that the variate displays for values of the variate less than or equal to the stated value of the variate. (See Figure 1b.)

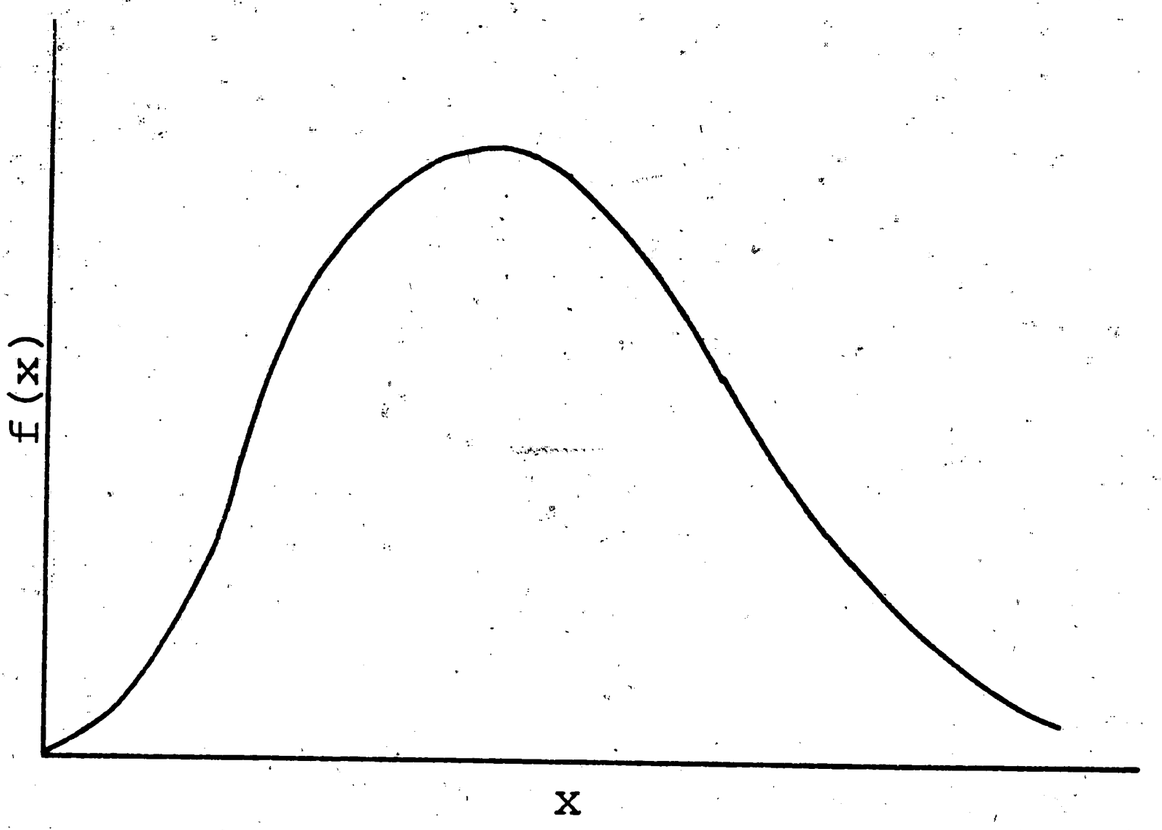

(a) probability distribution

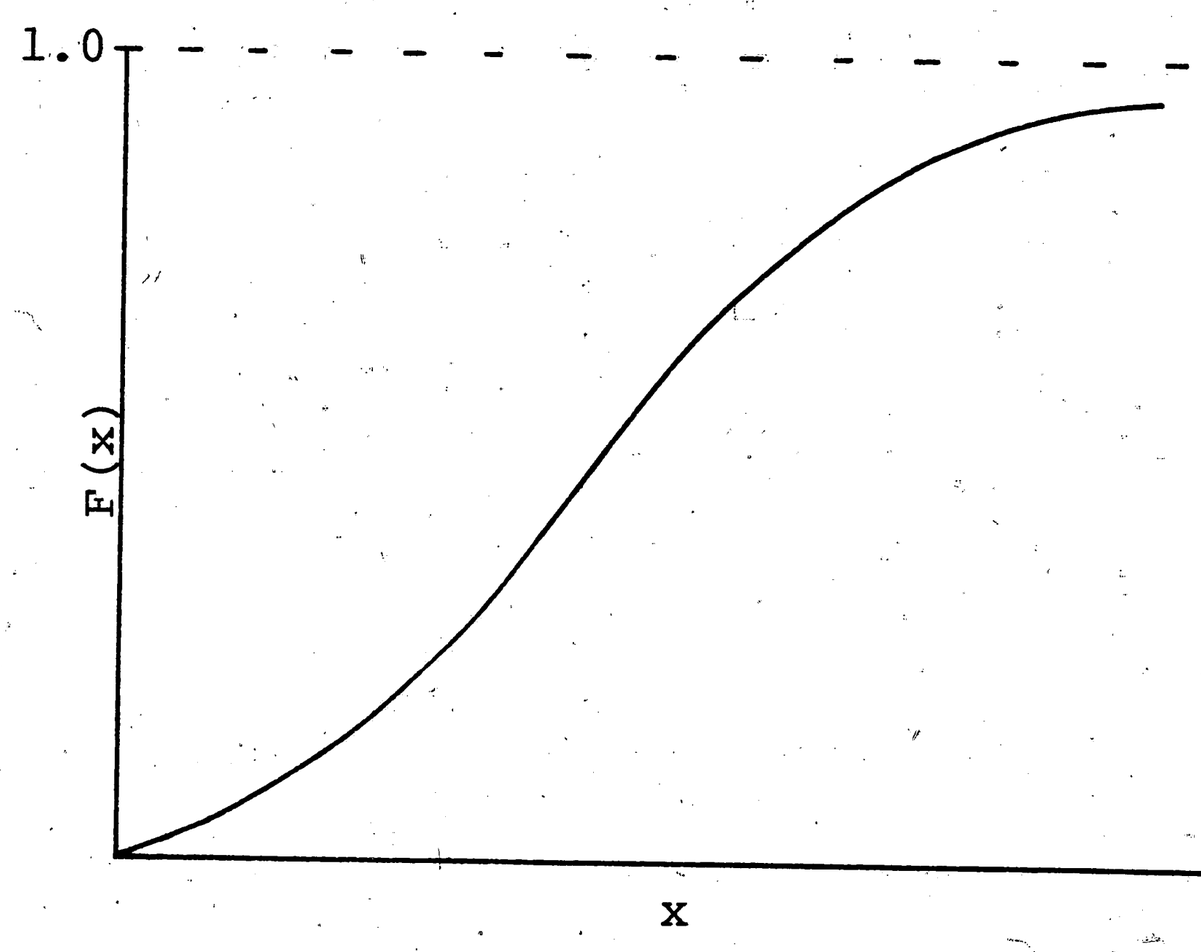

(b) cumulative probability distribution

Figure 1. Probability functions.

10) total probability for mutaully exclusive events - The total probability for two mutually exclusive events A and B is equal to the sum of the individual probabilities of occurrence. If p(A) = a and p(B) = b, then p(A or B) = a + b.

11) multiplicative law for independent events - As the title indicates, the probability of occurrence of two independent events A and B is equal to the probability of one event multiplied by the probability of the other. If p(A) = a and p(B) = b, then p(A and B) = ab.

These definitions and laws are fairly straightforward and largely self-explanatory. It should be noted, however, that throughout this section the terms probability and relative frequency are constantly interchanged. This assumes that a limiting value of relative frequency exists for each event of interest.

Constant Superheat Temperature Results as a Tool

If a fluid is subjected to a constant superheat at time zero, it is logical that as time goes by the cumulative probability of experiencing inception will increase from zero to one--one being the limit at time approaching

infinity. It is also reasonable that if the same fluid is subjected to a higher constant superheat, the cumulative probability of inception will increase at a faster rate and remain above that of the lower superheat. These concepts are pictured in Figure 2.

Two sets of additional curves may be derived from the cumulative curves: 1) the probability distribution curves and 2) the curves describing the cumulative probability of non-inception as functions of time. These curves are shown in Figures 3 and 4. To obtain the probability distribution for inception, or the probability of having an occurrence at a particular time, it is necessary to differentiate the cumulative curves. Note that the nature of the distribution curve indicates that a finite slope is assumed to exist for each cumulative curve at time approaching zero.

The cumulative probability of non-inception is arrived at by realizing that the cumulative probability of two mutually exclusive events is equal to one. Thus, the curves are calculated by subtracting the cumulative probability of inception from 1.0.

Both families of curves are fundamental to later calculations. Assuming that such patterns exist we may use them along with the multiplicative law to predict the

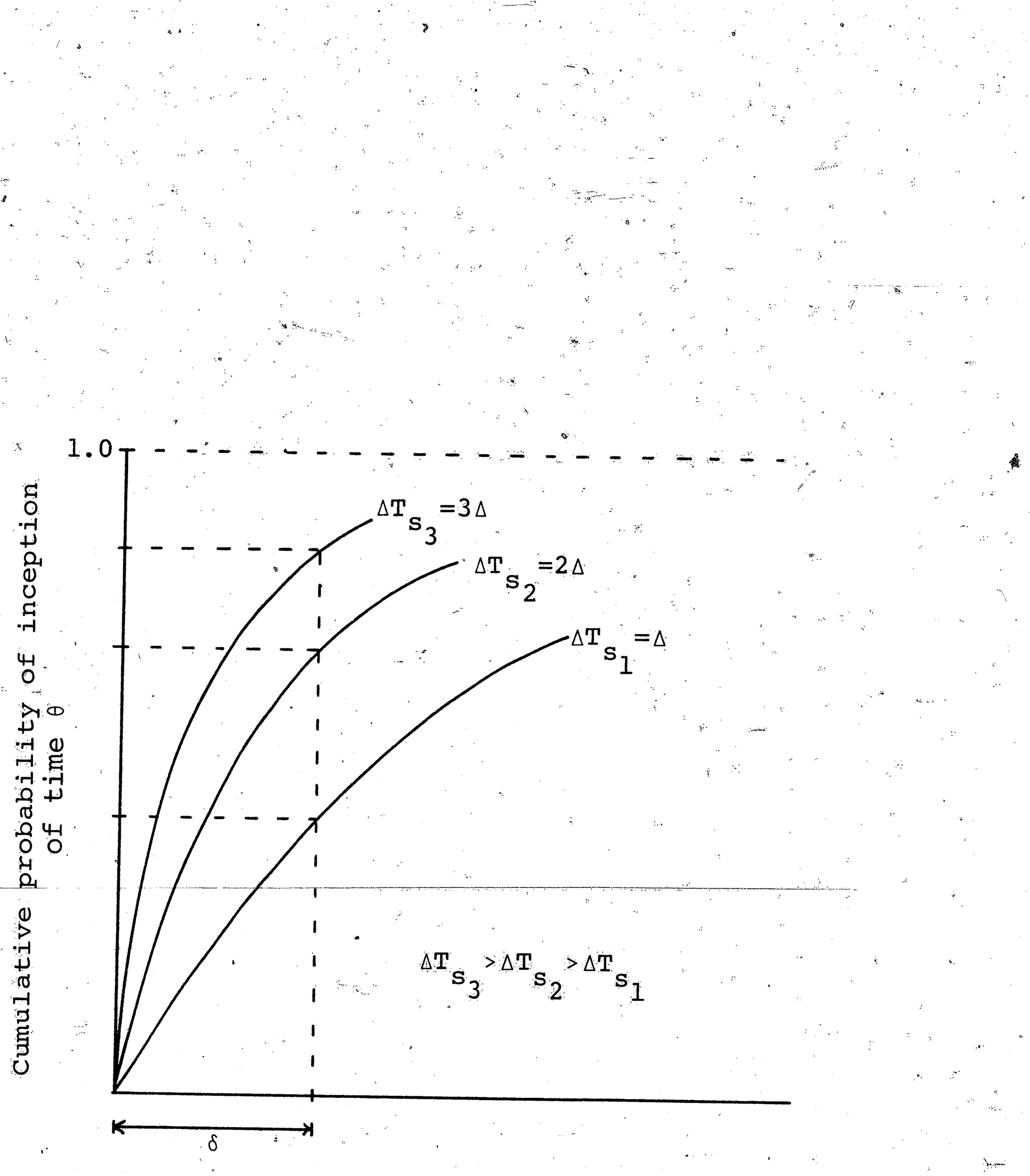

Figure 2. Cumulative distribution for inception.

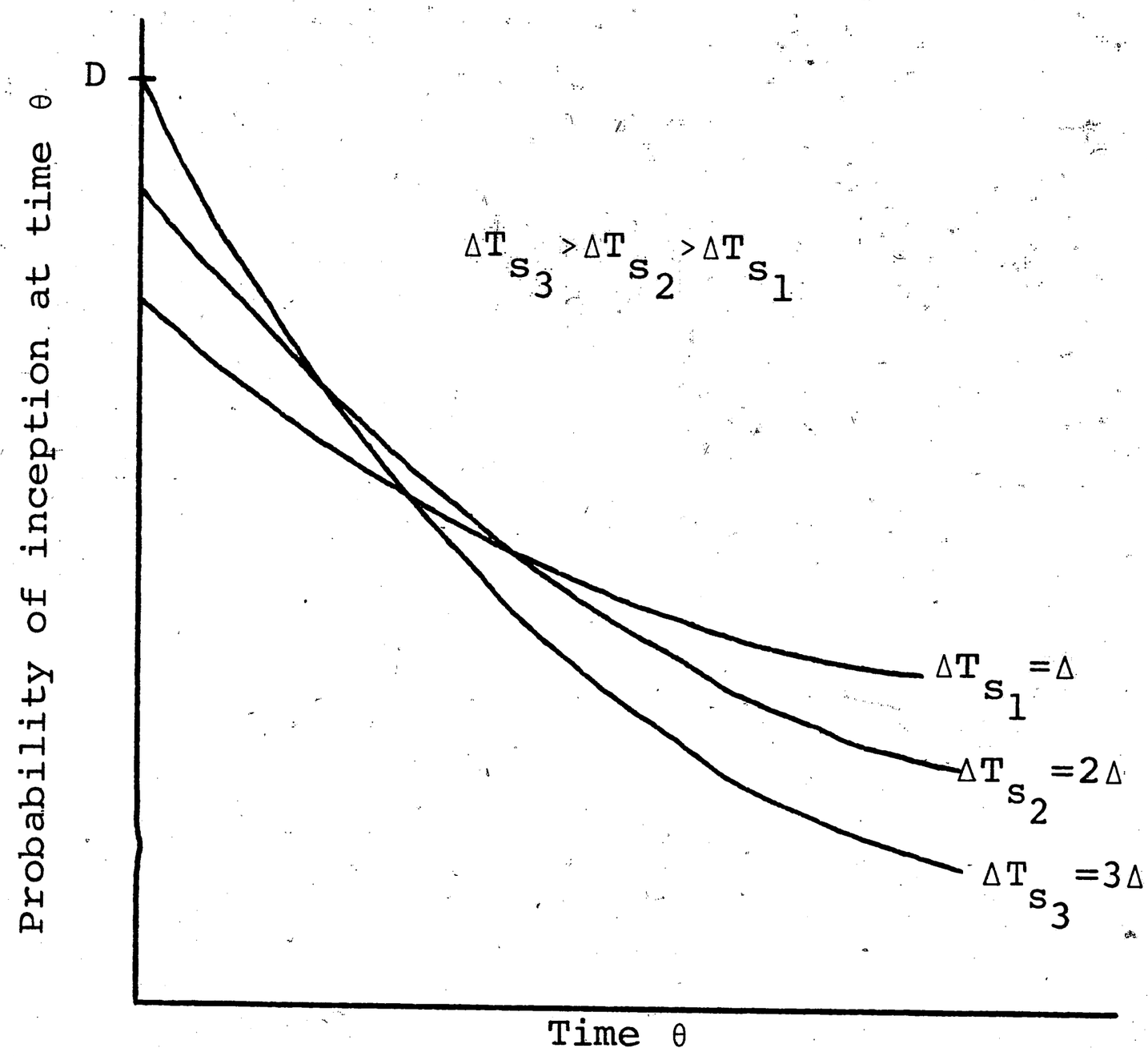

Figure 3. Probability distribution for inception.

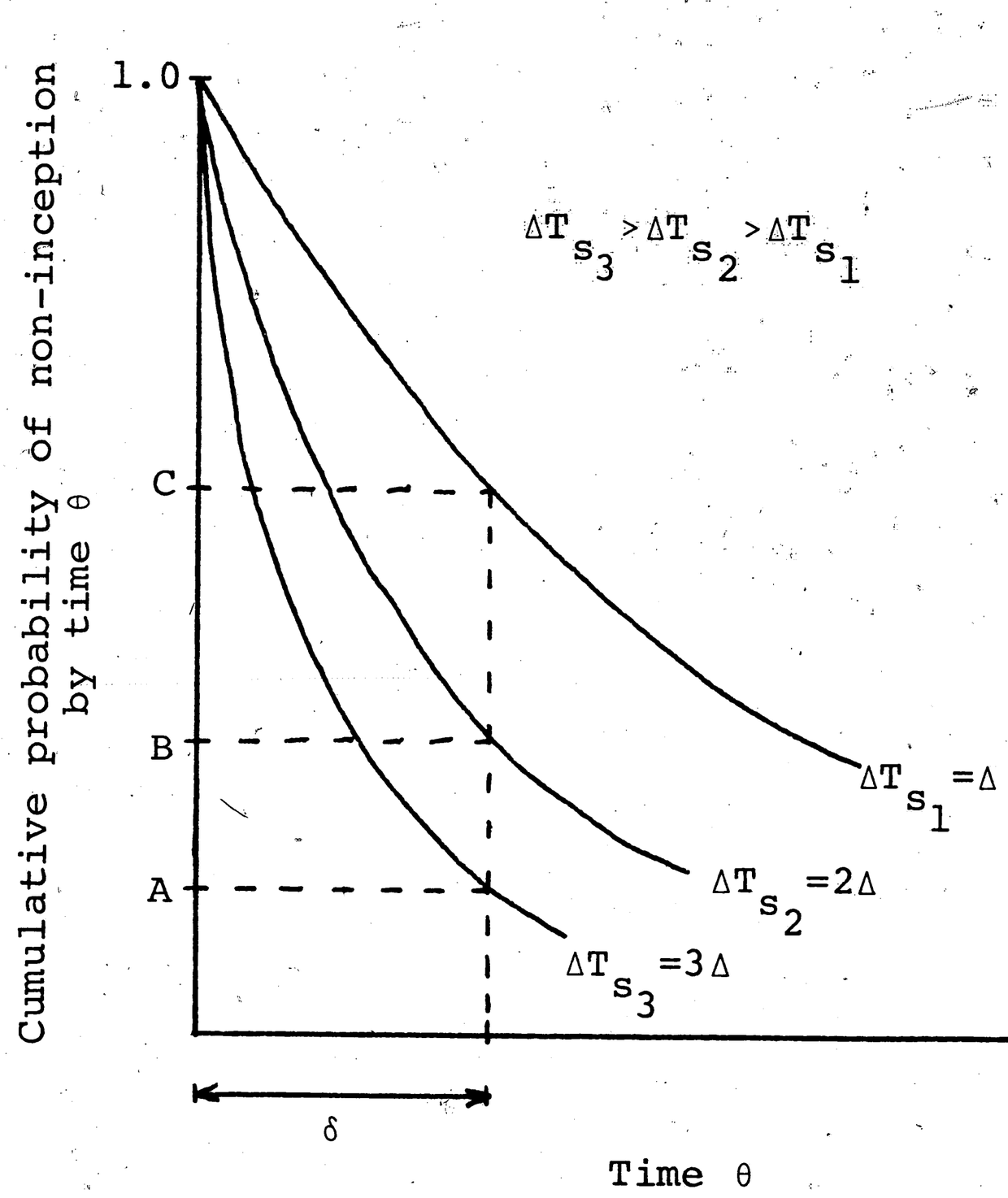

Figure 4. Cumulative distribution for non-inception.

most probable superheat at inception for a fluid that is experiencing a constant temperature ramp.

Use of Constant Temperature Results to Predict Constant Temperature Ramp Results

It is possible to approximate a temperature ramp by a series of uniform steps, each characterized by a temperature increase Δ and a time interval δ. Such a ramp is shown in Figure 5.

If we are interested in determining the probability of inception at point P, we may quickly do so if uniform temperature data is available in the form of cumulative probability curves for each temperature step involved. This data may be reduced as described previously to yield all necessary information for the problem. (See Figures 2, 3, and 4.)

The probability of an occurrence at P is a function of what happens at θ_p and the history from time zero until θ_p. Statistically, it is equal to

(probability of no inception during an interval of time δ at a superheat Δ) $\times$ (probability of no inception during an interval of time δ at a superheat 2Δ) $\times$ (probability of no inception during an interval of time δ at a superheat 3Δ) $\times$ (probability of inception during an infinitesimal time interval at a superheat 3Δ).

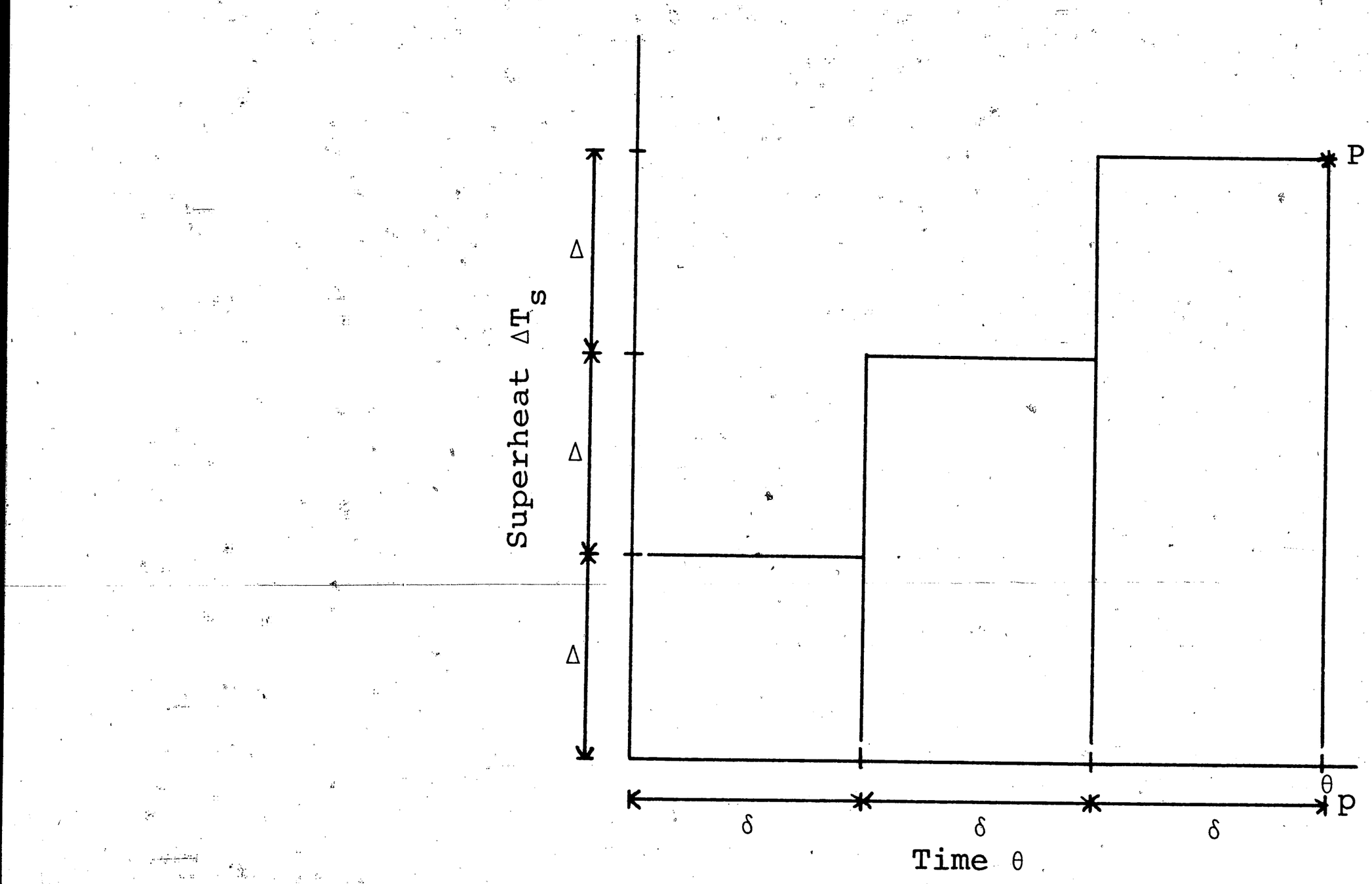

Figure 5. Approximation of a temperature ramp using incremental steps.

These values are available from Figures 3 and 4; therefore, the probability of inception at point P = (A)(B)(C)(D).

Point P is not a fixed point, but can be shifted anywhere along the approximate staircase for a particular ramp; or it may be shifted along any other staircase approximating a different temperature ramp. The limiting quantity in this process is the number and spacing of the cumulative probability of inception curves available for uniform superheat temperatures.

The values of probability calculated in this manner can then be graphed to show the relationship between superheat and probability of inception as a function of temperature ramp. This information, pictured in Figure 6, indicates the most probable superheat at inception for each ramp rate, shown in Figure 7. It should be noted that as temperature ramp rate increases, there will be a flattening out of the curve, and the range of superheats having probabilities close to the maximum increases. Thus, it would be expected that scatter in experimental results would tend to increase with temperature ramp.

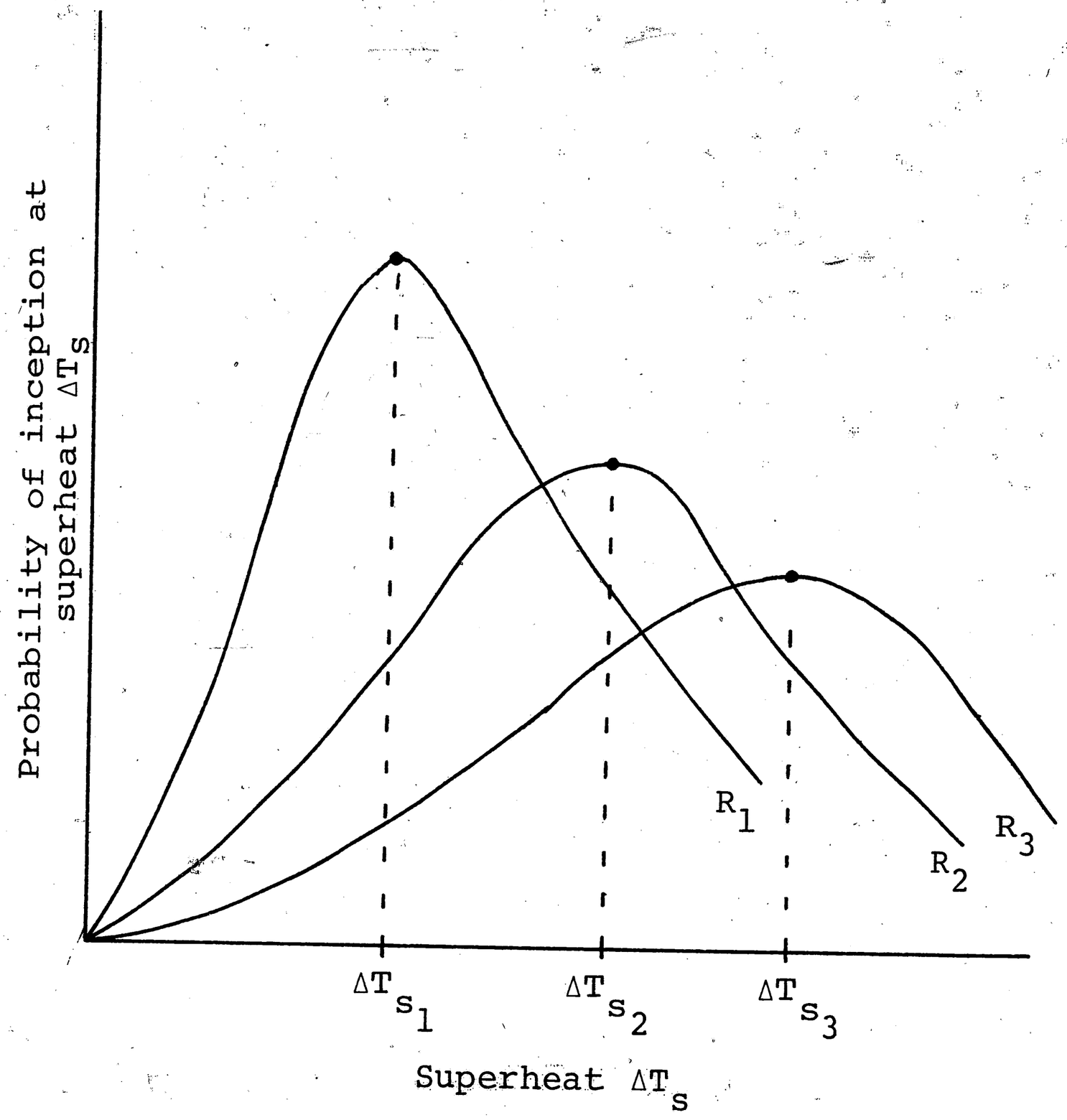

Figure 6. Derived probability distribution for inception.

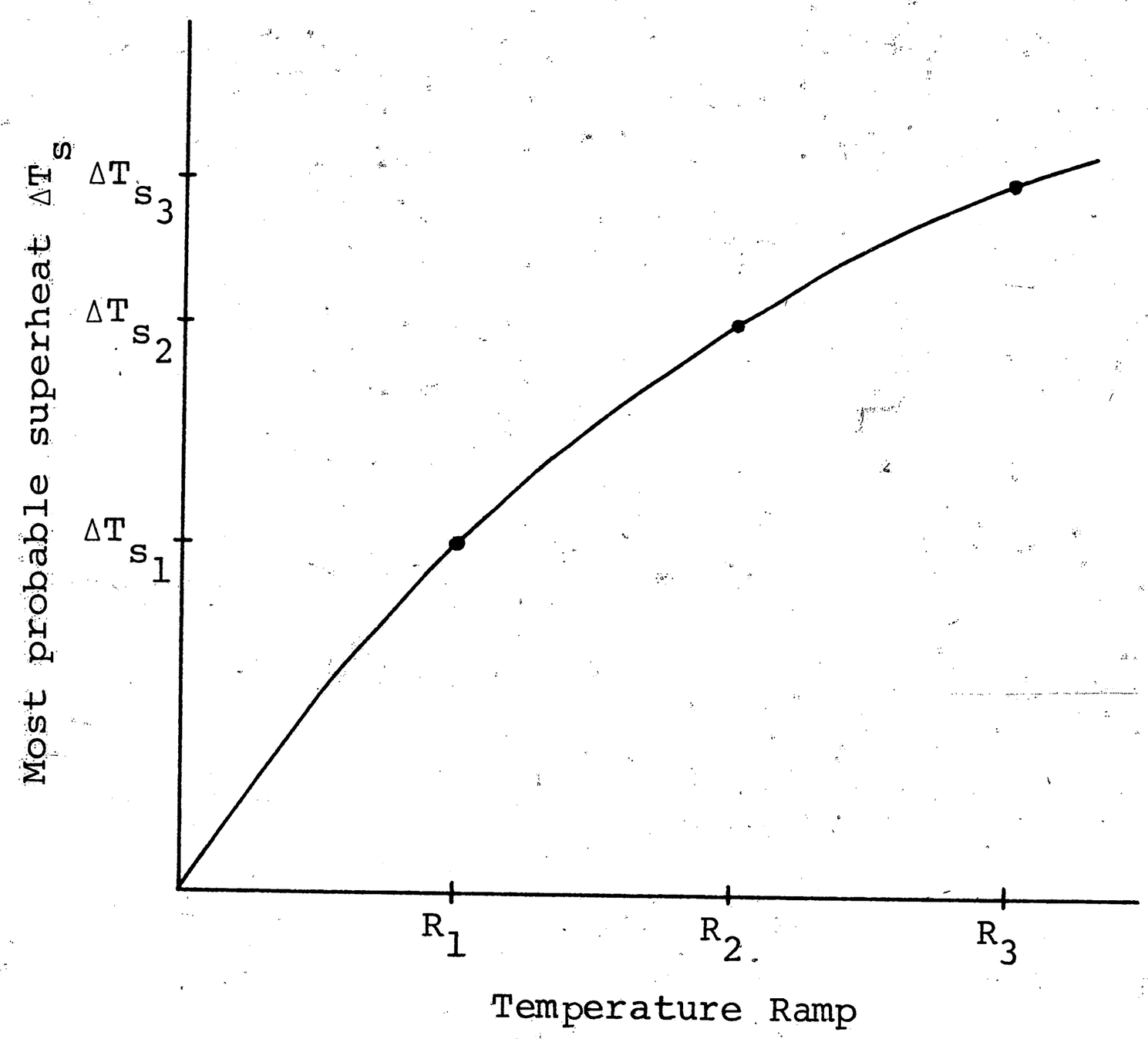

Figure 7. Derived values of most probable superheat.

EXPERIMENTAL FINDINGS IN SUPPORT OF A STATISTICAL THEORY

General Information

To facilitate experimentation it was first necessary to find a fluid capable of sustaining superheat which did not require elaborate or expensive equipment. Freon 113 (trichlorotrifluoroethane) seemed to be the only fluid which fit these requirements, although it was not known just how much superheat could be expected. While the experiment was in the fabrication stage, however, a paper to be presented at the 1972 Heat Transfer and Fluid Mechanics Institute was reviewed. The paper--submitted by Murphy and Bergles [1]--dealt with subcooled flow boiling of fluorocarbons and indicated that superheats on the order of 30°F had been obtained. Thus, it was realized that a much greater range of superheats was available than had been previously anticipated.

After an abortive, complicated attempt the apparatus involved in the tests was considerably simplified. Basically, the elements included were:

1) a glass test tube containing a fluid specimen whose temperature could be recorded
2) an engineering surface where inception would occur
3) a water bath whose temperature could be regulated

4) a discharge system to capture fluid boiled off.

Figure 8 shows all components involved.

The temperature measurement of the Freon sample was taken by an iron-constantan thermocouple attached to the outer wall of the glass tube. To reduce the temperature gradient across the tube wall at the thermocouple position, a glob of silicone seal was used to insulate the couple. In this case the temperature measured by the thermocouple was a close approximation to the fluid temperature inside the tube. This procedure is demonstrated in Figure 9.

The engineering surface used to foster inception was a small ball bearing. The surface proved reliable, and all test inceptions occurred at the bearing surface unless otherwise noted.

The water bath was heated by a hot plate and a heating tape coiled around the bath. These were regulated by variac controllers. To ensure that temperature gradients did not exist in the bath, a mixer was incorporated and maintained at a constant speed throughout the testing.

A water jacket condenser unit was used to condense boiled out Freon vapor, and a vented collection bottle captured the liquid for use in future work.

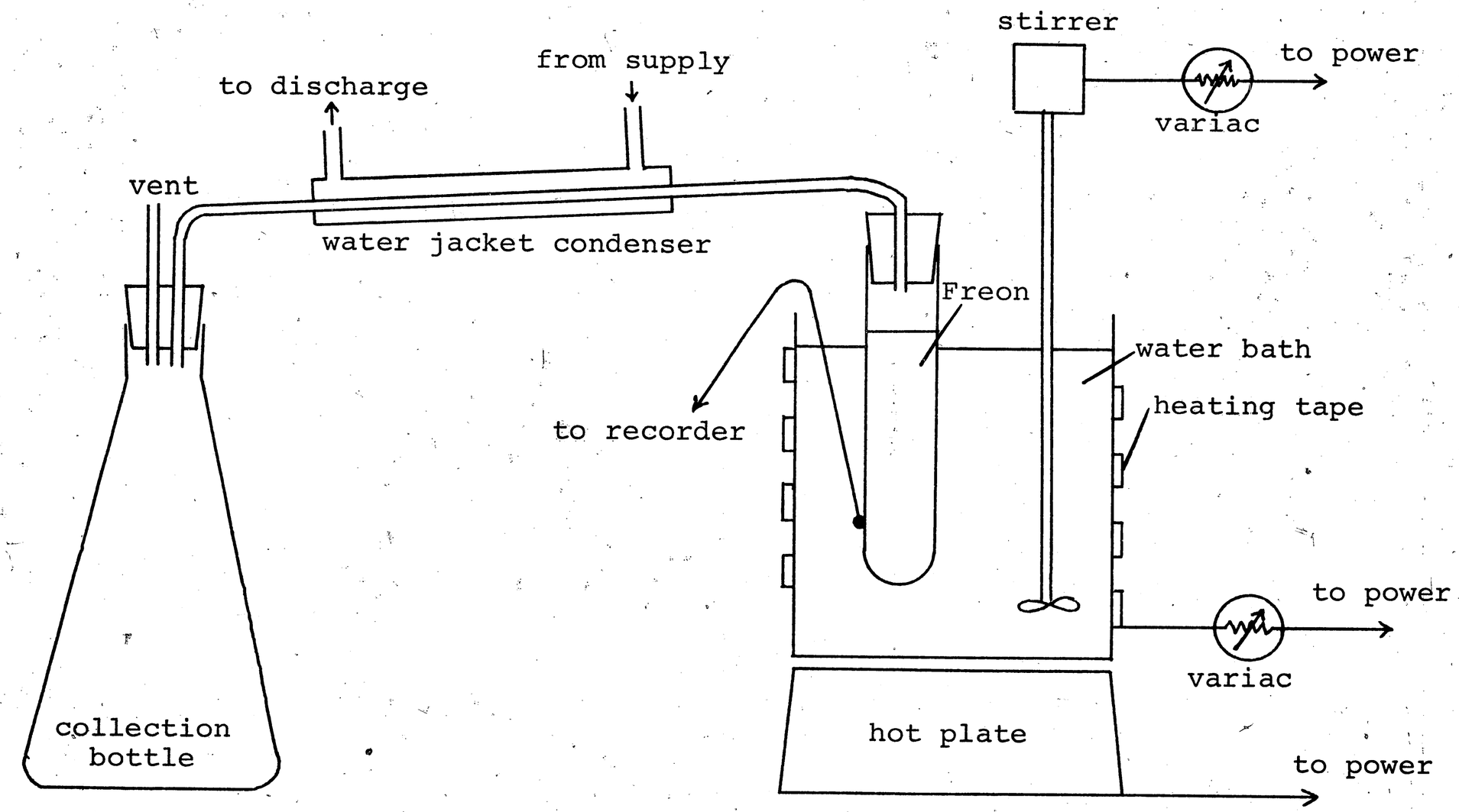

Figure 8. Experimental apparatus.

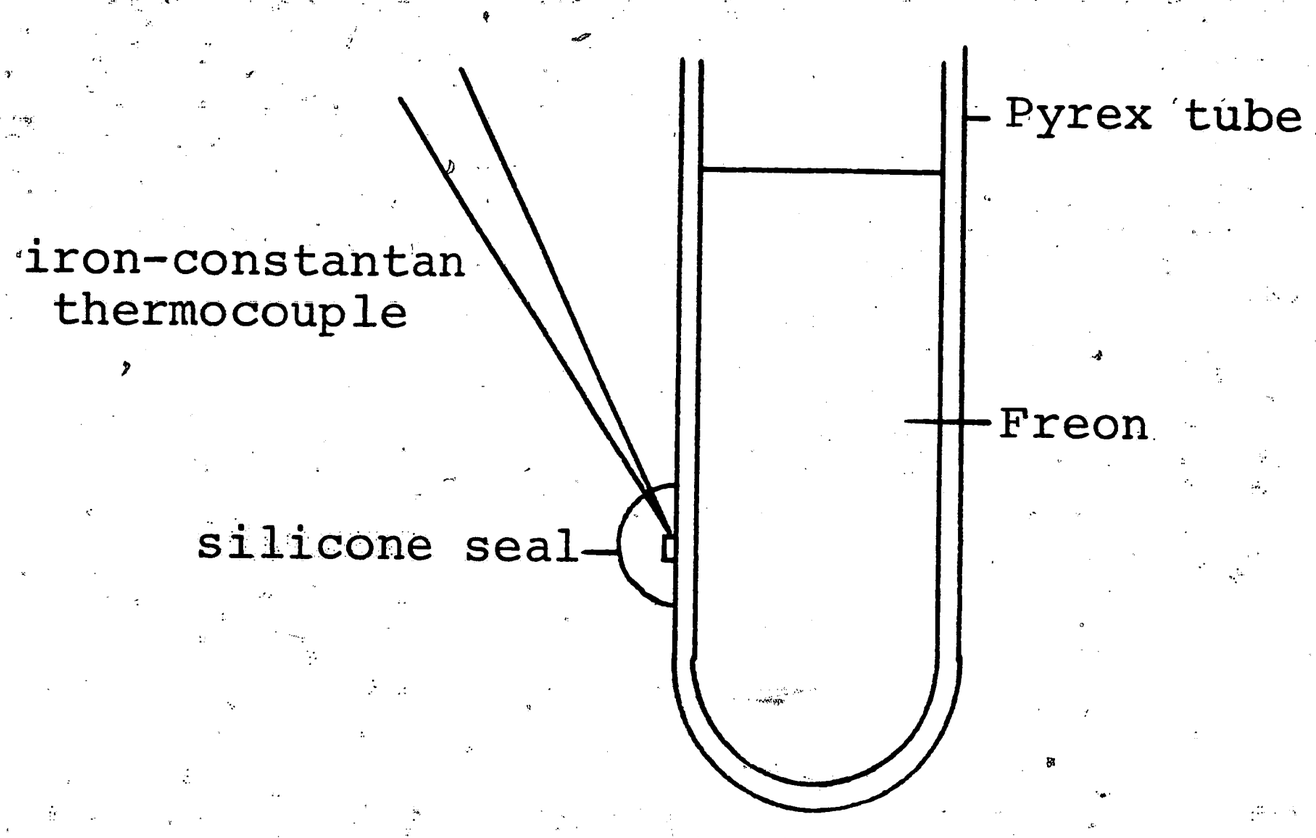

(a) tube detail

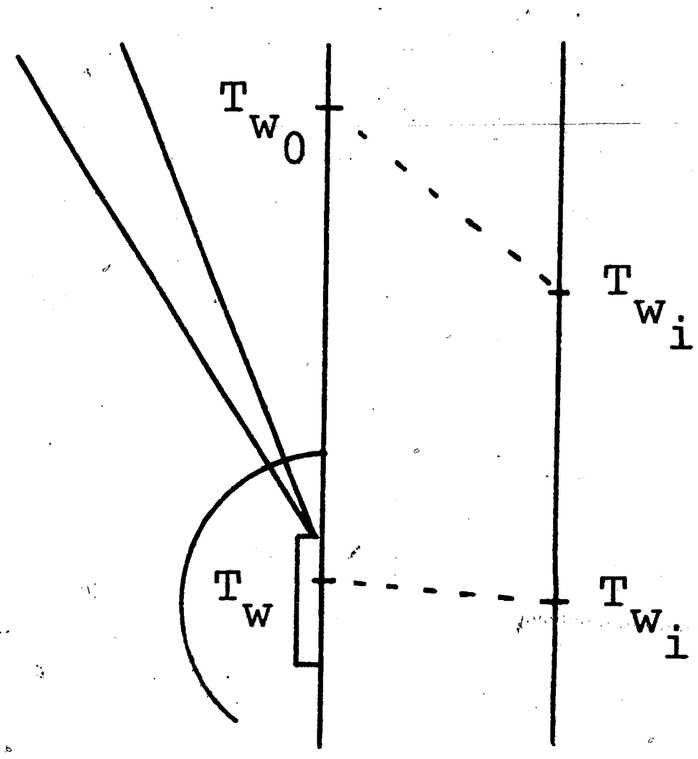

(b) temperature measurement detail

Figure 9. Temperature measurement information.

In general all tests were conducted with the same equipment. Due to the nature of the problem it was important that this was the case. Early tests indicated that inception would be influenced by the size and surface condition of the bearing, the surface of the sample tube, and the stirrer speed and vibration as noticed through motion of the bearing and fluid in the test tube.

Degassing and Deactivation

Each test incorporated two special procedures dealing with degassing of the fluid sample and deactivation of available sites for inception.

Superheat is highly influenced by the amount of dissolved gas in the liquid. Early methods used to remove gas involved boiling the sample for some minimum time to release dissolved gas and to create a Freon vapor atmosphere over the surface. These methods, however, required a great deal of time and Freon, and they were abandoned in favor of a simpler, more repeatable process.

Since the amount of dissolved gas in Freon is a strong function of how much air the fluid "sees," it was desirable to reduce the air-Freon contact to a minimum. To facilitate this a large supply bottle was devised so that a siphon tube which ran from the bottom of the bottle to the bottom of the test tube could be used to re-supply

the sample tube at the start of each trial. Thus a minimum and constant amount of Freon was exposed to air; and, hopefully, the quantity of dissolved gas in each sample was also minimum and constant.

Deactivation of available sites for inception is also believed to play a large role in determining what superheat is attainable in the fluid. For the experiments it was necessary only to standardize deactivation procedures to remove one more variable from the process.

Deactivation is thought to be primarily a function of temperature: the lower the pre-test temperature, the smaller the size of sites which are effectively deactivated, or flooded. The standard procedure adopted for the tests involved a fifteen minute pre-soak of the sample and tube in a 70°F bath. Detailed procedures for both ramp and step tests may be found in the Appendix.

Constant Temperature Ramp Tests

As has been previously stated, the procedure for the inception tests involving a constant temperature increase per unit time in the region of superheating is described in the Appendix. It is necessary, however, to be aware of the conditions and nomenclature of the tests to properly interpret the results. Figure 10 indicates information of value; specifically, how superheat at

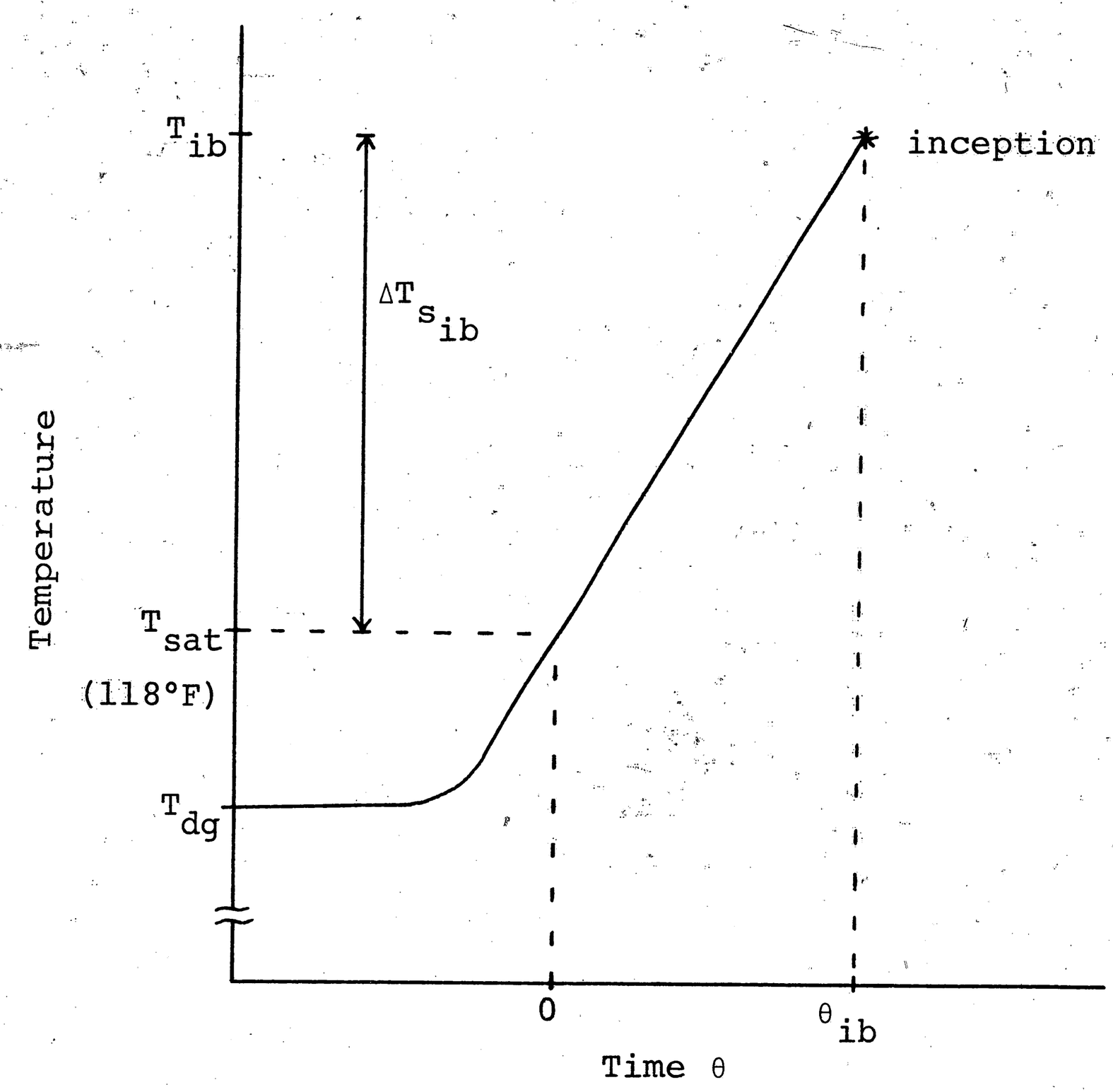

Figure 10. Ramp test nomenclature.

inception and time at inception are evaluated for a ramp test.

Figures 11, 12, and 13 give the actual experimental results of all ramp tests undertaken. These results were systematically evaluated to remove data points which were considered to be unacceptable for analysis. A "standard inception" refers to the fact that inception occurred at the bearing surface; "other inception" refers to inceptions from various wall sites in the tube or at different positions in the fluid. The cause of non-standard inceptions was strongly related to the nature of the test system: the surface being heated directly was not the surface from which standard inception occurred. Since temperature gradient is an important factor influencing inception, the number of "other inceptions" increased markedly as temperature ramp increased.

"Standard procedure" refers to methods detailed in the Appendix; "other procedure" refers to several early tests in which a slightly different deactivation procedure was used. However, since the deactivation temperature was the same for both procedures, the results were included as acceptable.

"Last experiments" indicates the results of the last day of testing, which yielded such significantly

Figure 11. Ramp test results--all tests.

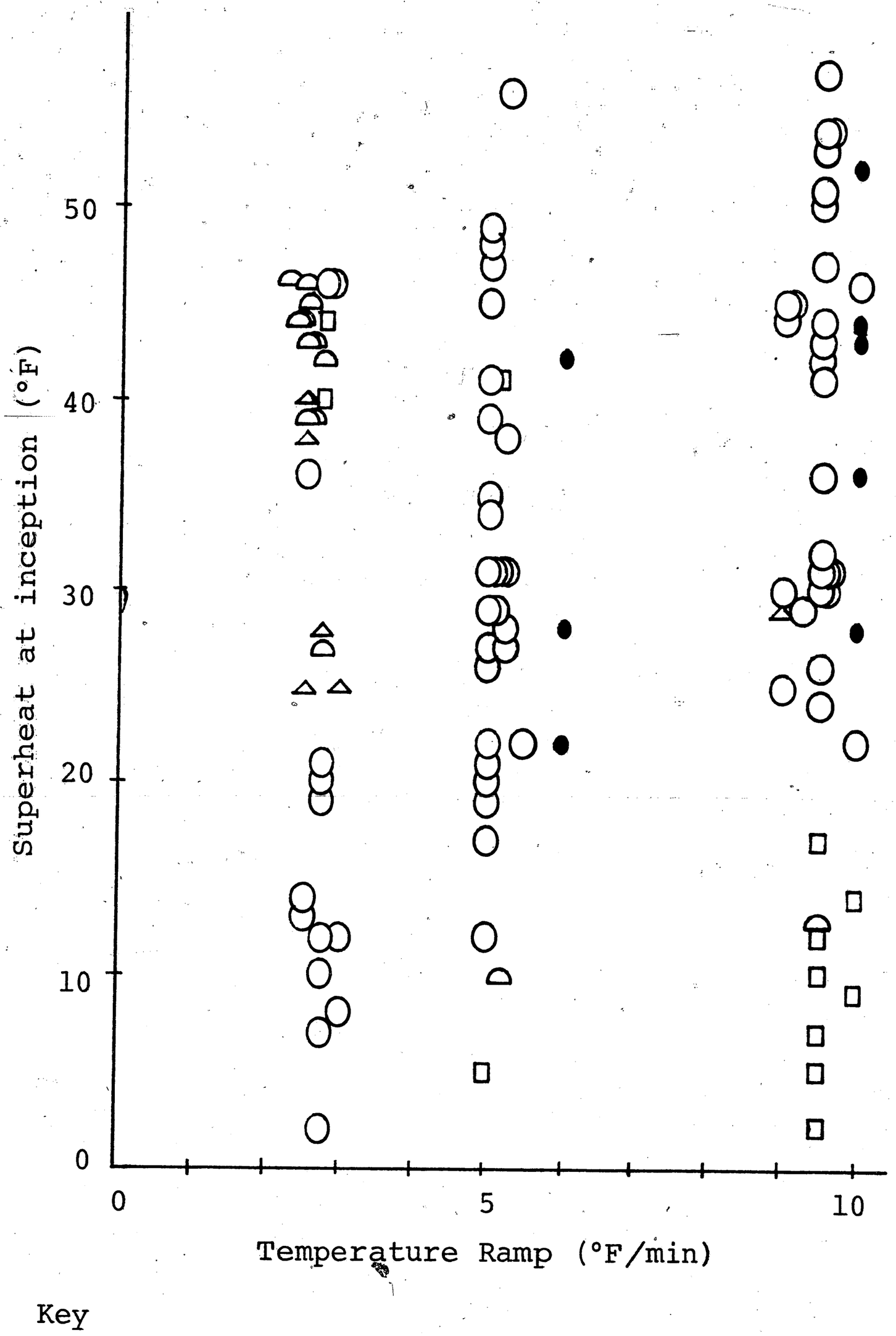

Key

- ○ standard procedure, standard inception
- ● other procedure, standard inception
- □ standard procedure, other inception
- △ standard procedure, standard inception, last experiments
- ◠ standard procedure, other inception, last experiments

Figure 12. Ramp test results--excluding last experiments.

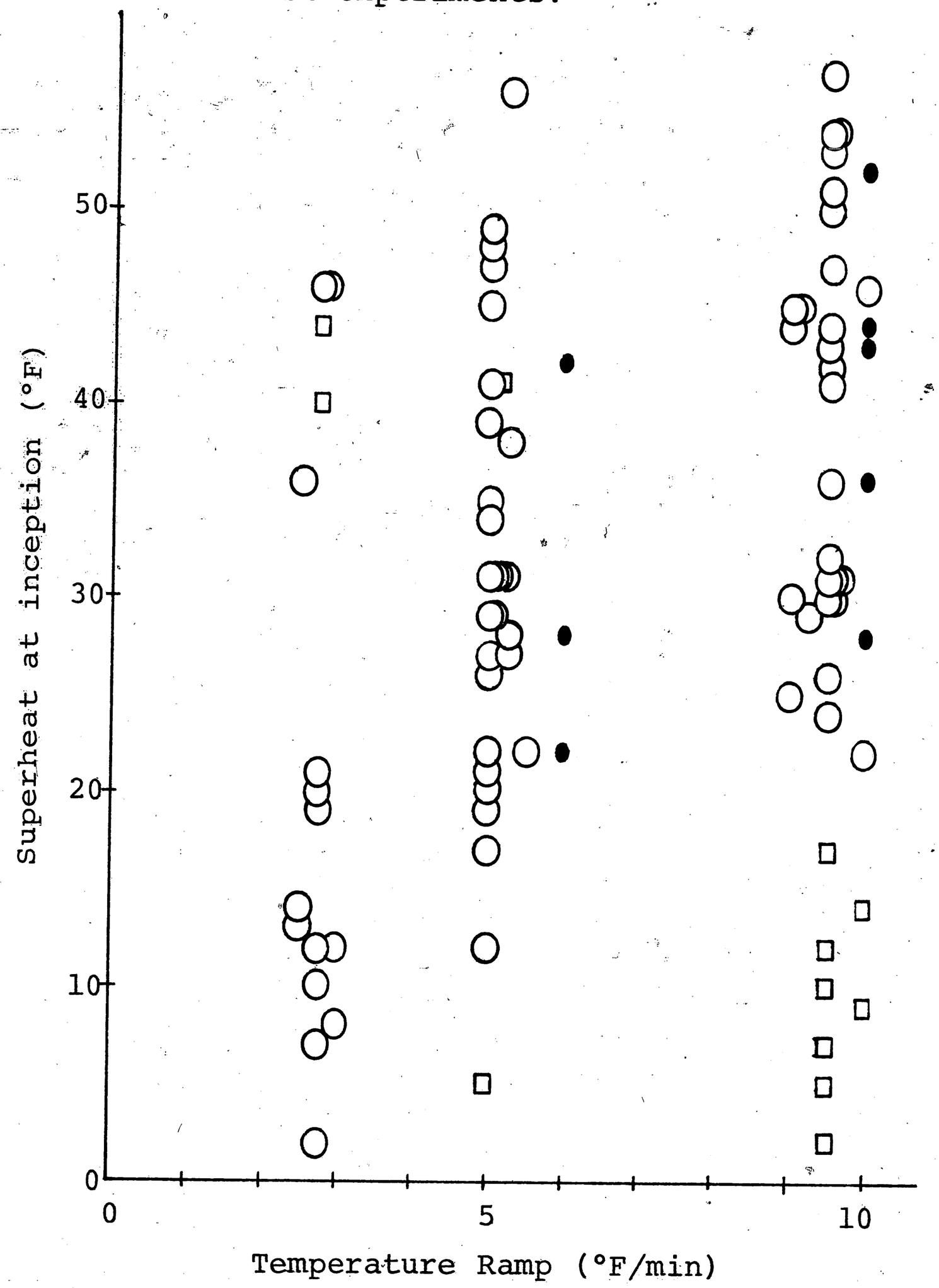

Key

- ○ standard procedure, standard inception
- ● other procedure, standard inception
- □ standard procedure, other inception

Figure 13. Ramp test results--acceptable tests.

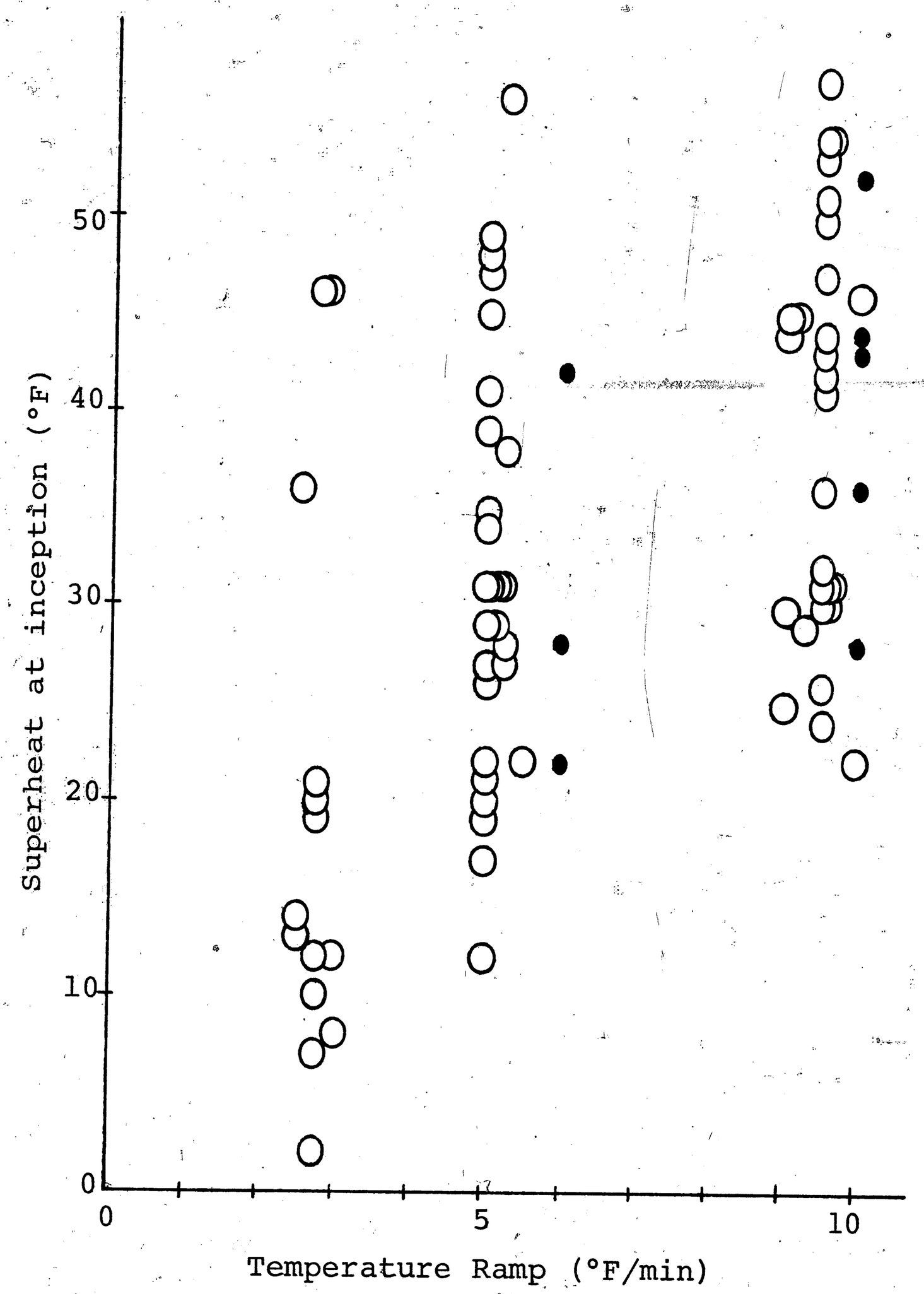

Key

○ standard procedure, standard inception

● other procedure, standard inception

deviant results that all results for the day were excluded. Figure 13 shows the results which were finally considered acceptable for further analysis.

The acceptable results were then graphed for each temperature ramp with the ordinate being the number of tests whose incipient superheat was less than or equal to the superheat specified by the abscissa. Figure 14 displays these graphs as well as the normalization of each, which is actually the cumulative probability of an inception as a function of superheat. These cumulative curves were then differentiated to yield probability distribution curves for each temperature ramp with the ordinate being the probability of inception at a particular superheat given by the abscissa. Figure 15 gives the curves for three temperature ramps on one set of coordinates.

The desired end results for these tests--the most probable superheat at inception for a given temperature ramp--may then be visually determined from the curves in Figure 15. These points are plotted in Figure 16.

Constant Superheat Step Tests

The detailed procedure followed when conducting a step test is given in the Appendix. Again nomenclature is necessary for understanding how the data has been evaluated. Figure 17 displays the general form of the

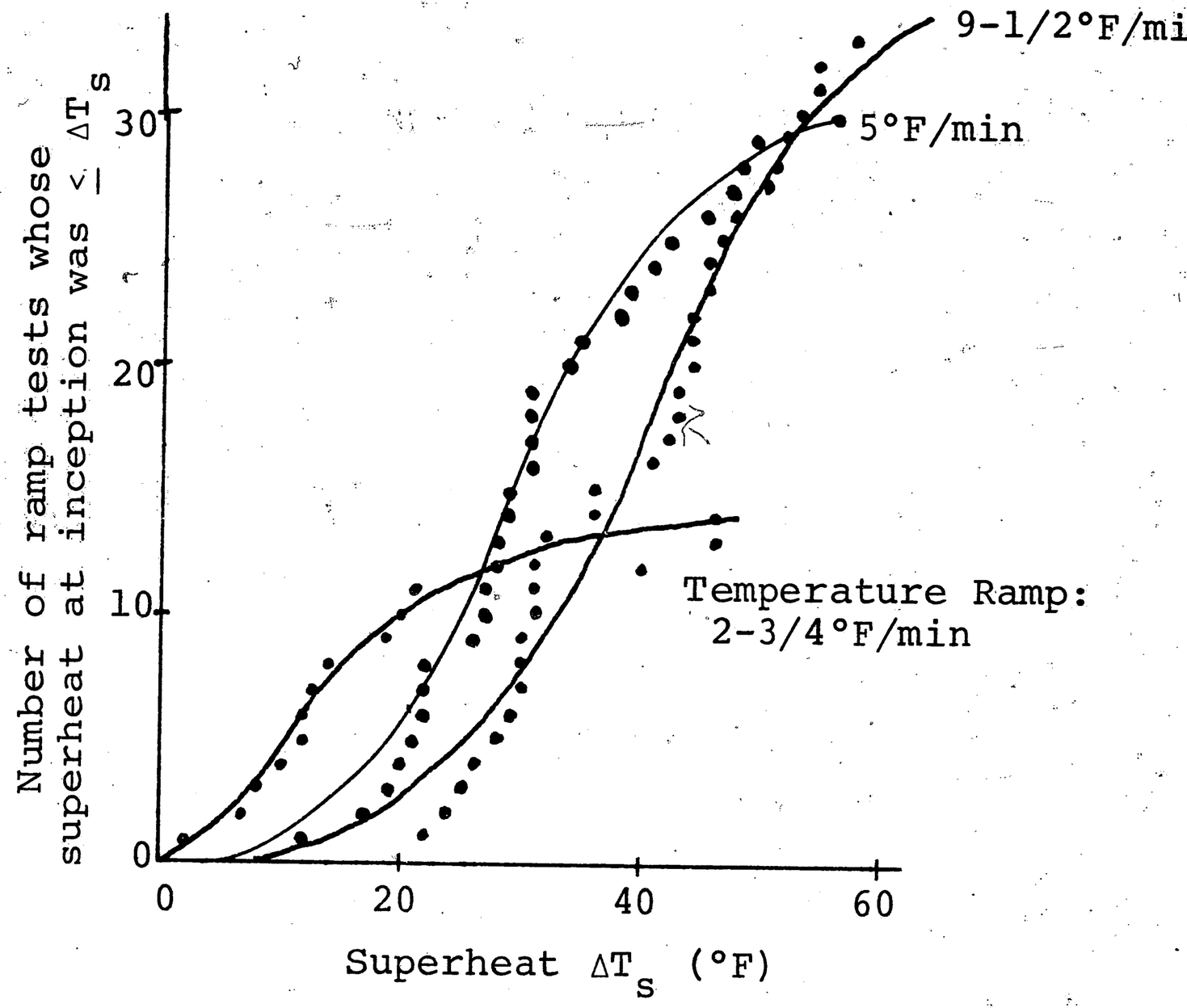

(a) accumulated inceptions

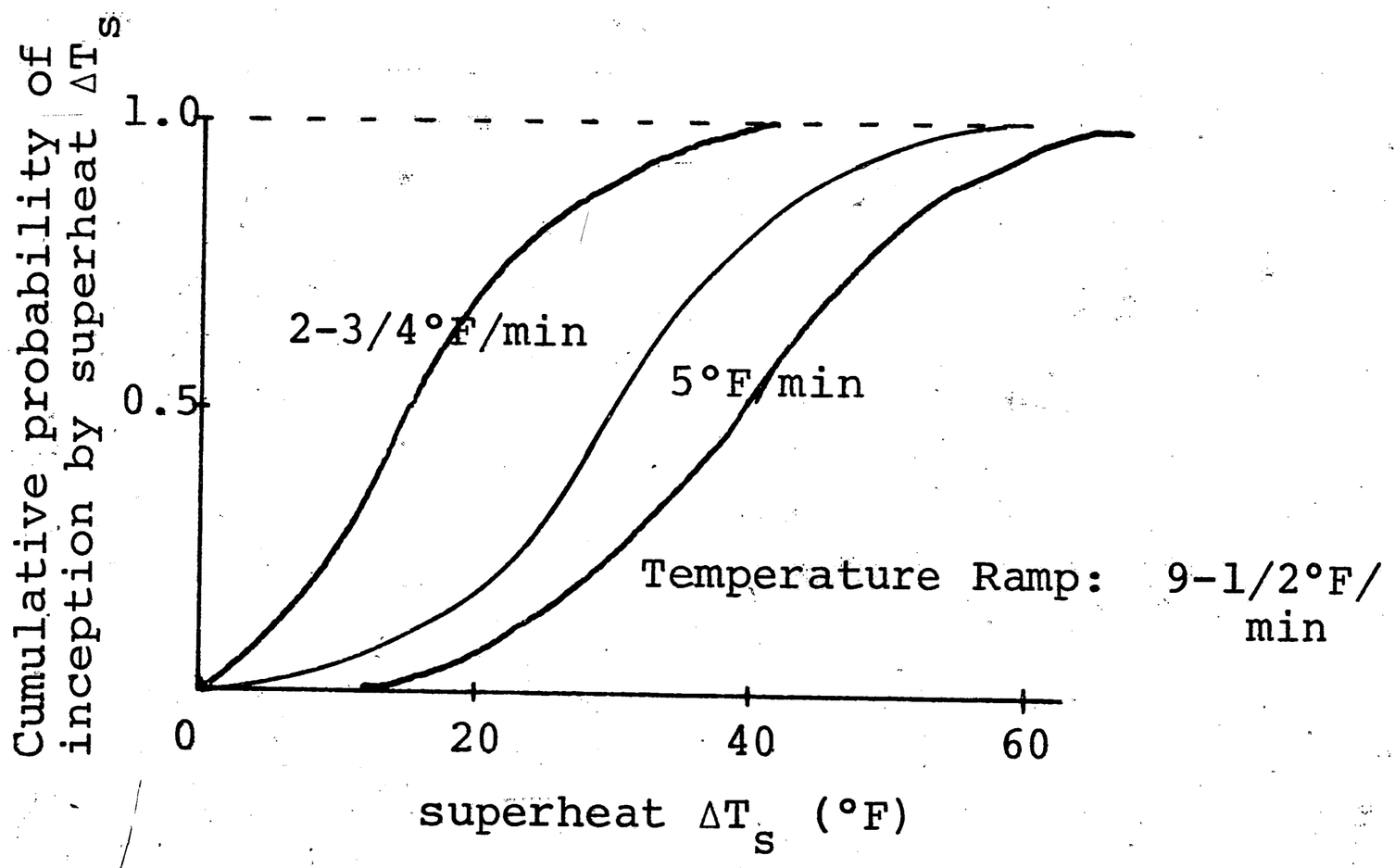

(b) normalized cumulative probabilities of inception

Figure 14. Ramp test results as accumulated probabilities.

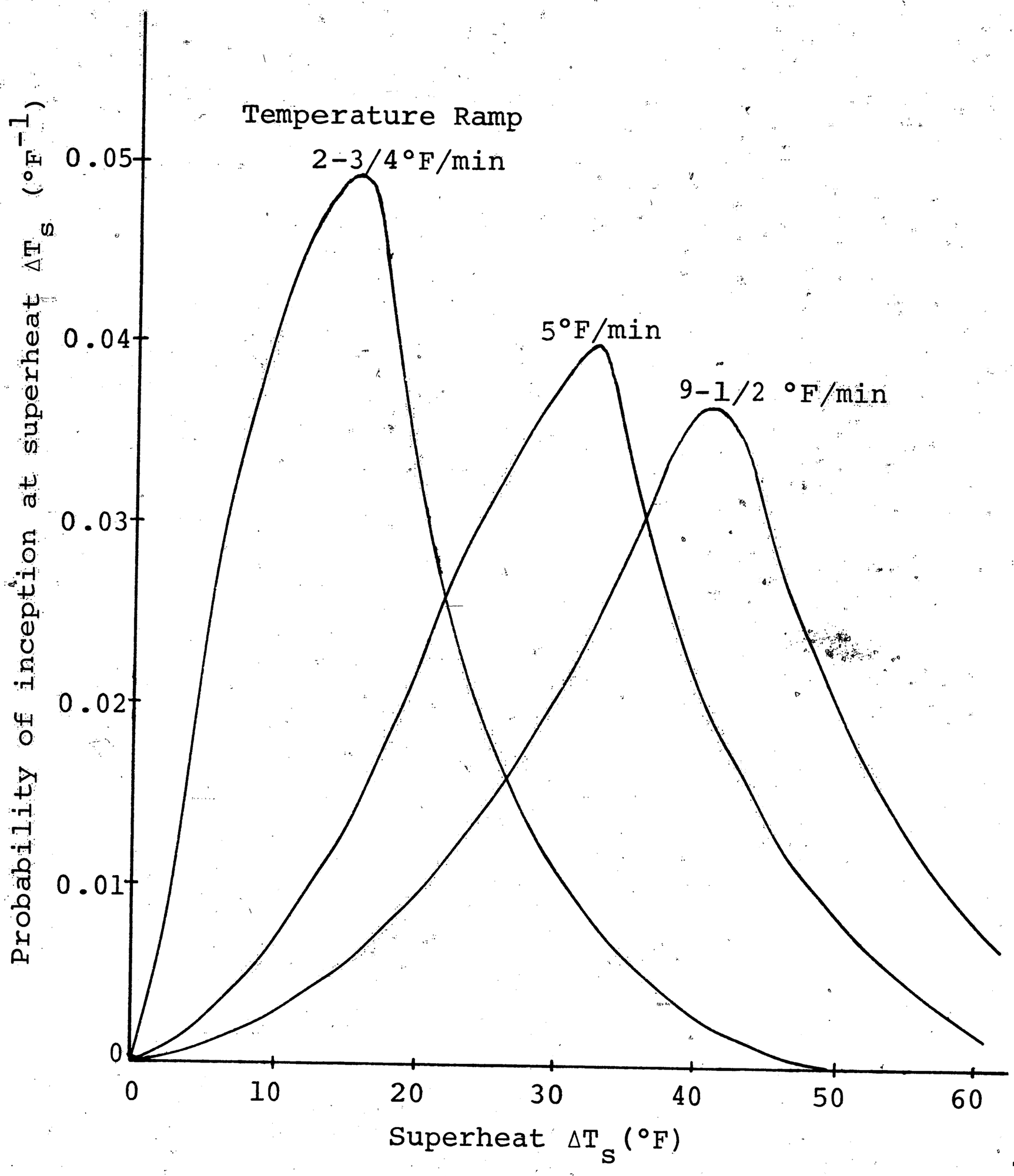

Figure 15. Probability distributions of inception determined from ramp test results.

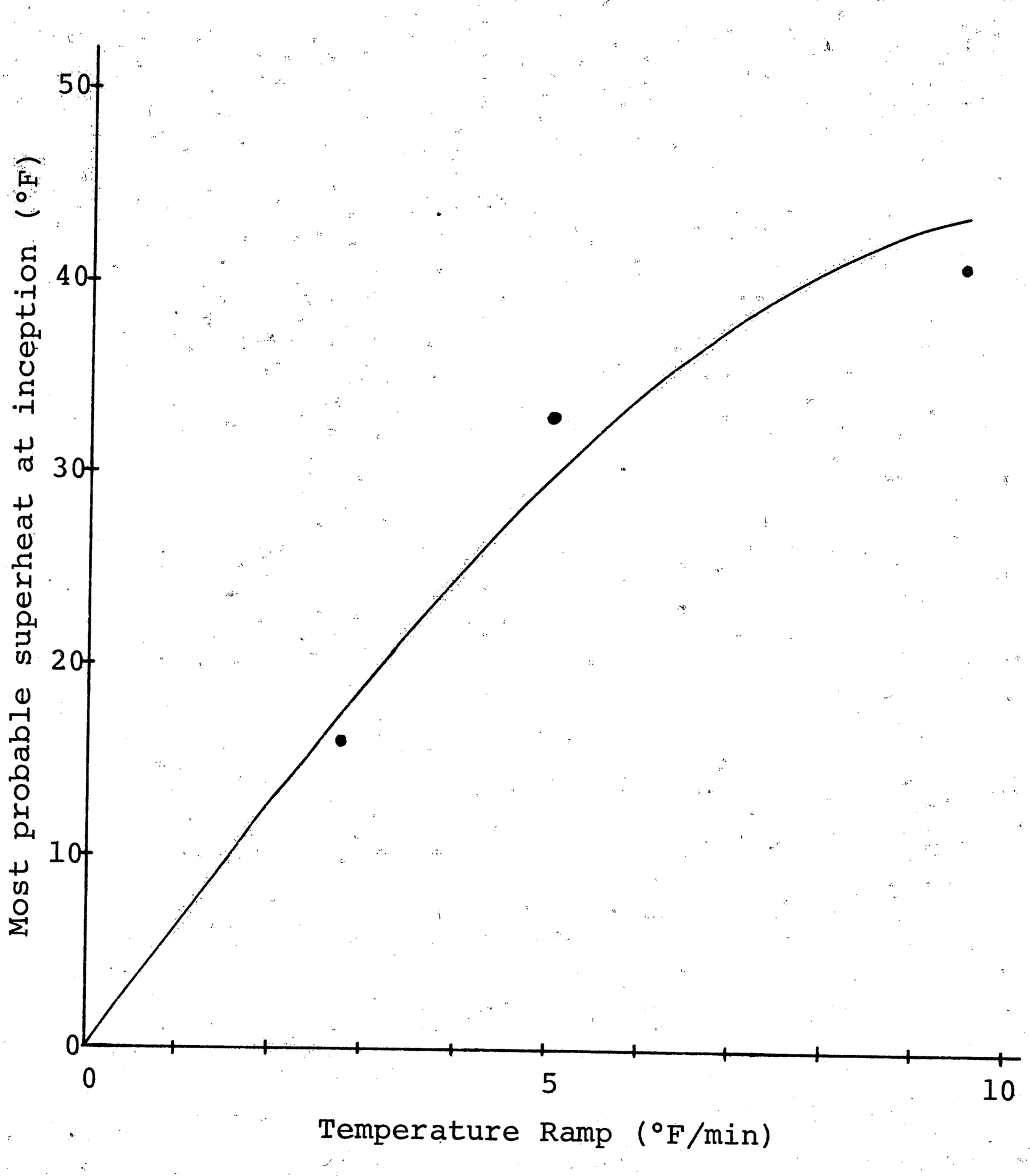

Figure 16. Experimentally determined relationship between most probable superheat and temperature ramp.

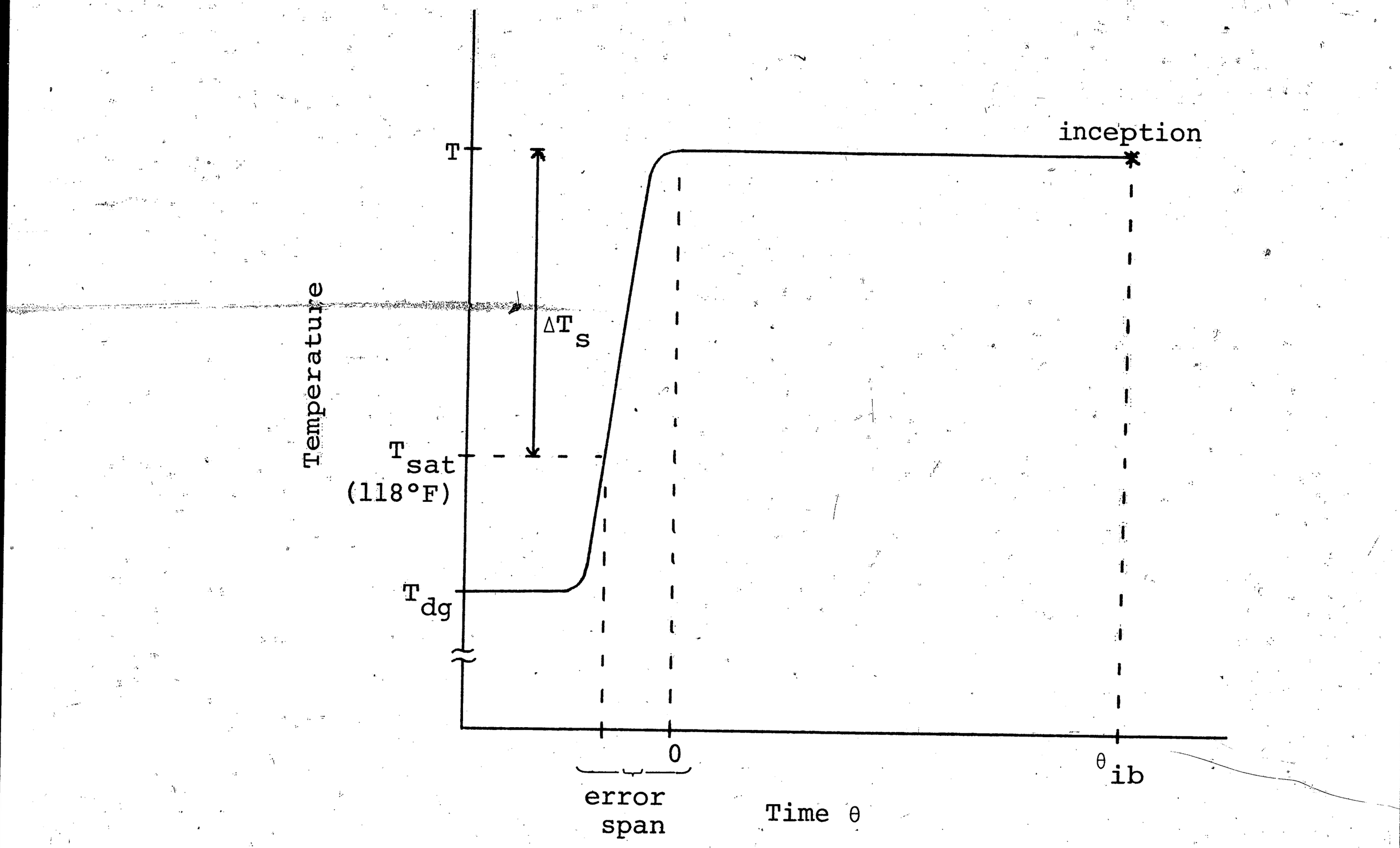

Figure 17. Step test nomenclature.

results recorded from the wall thermocouple in terms of time of inception and the superheat step. Because of the grossness of the experimental system it was not possible to apply a true temperature "step" to the specimen. In actuality a certain amount of time was required for the Freon sample to reach the test superheat. This time is noted as the "error span" in the figure and was generally about one and a half minutes.

Figure 18 shows the experimental results in graphical form of each of three superheats tested with the ordinate being the accumulation of number of tests which had experienced inception in time less than are equal to that value of time given by the abscissa. The blocks are included to allow for the region of uncertainty caused by the error span. These curves have been normalized into cumulative probability of inception curves in Figure 19. Note the presence of the dotted line cooresponding to each curve. These lines were included as a truer approximation of the curves in the region of time generally associated with the error span.

Earlier it was mentioned that ramp test results could be predicted from step test results if two families of curves were available: curves showing the cumulative probability of non-inception and the probability distribution of inception as functions of time. These curves have

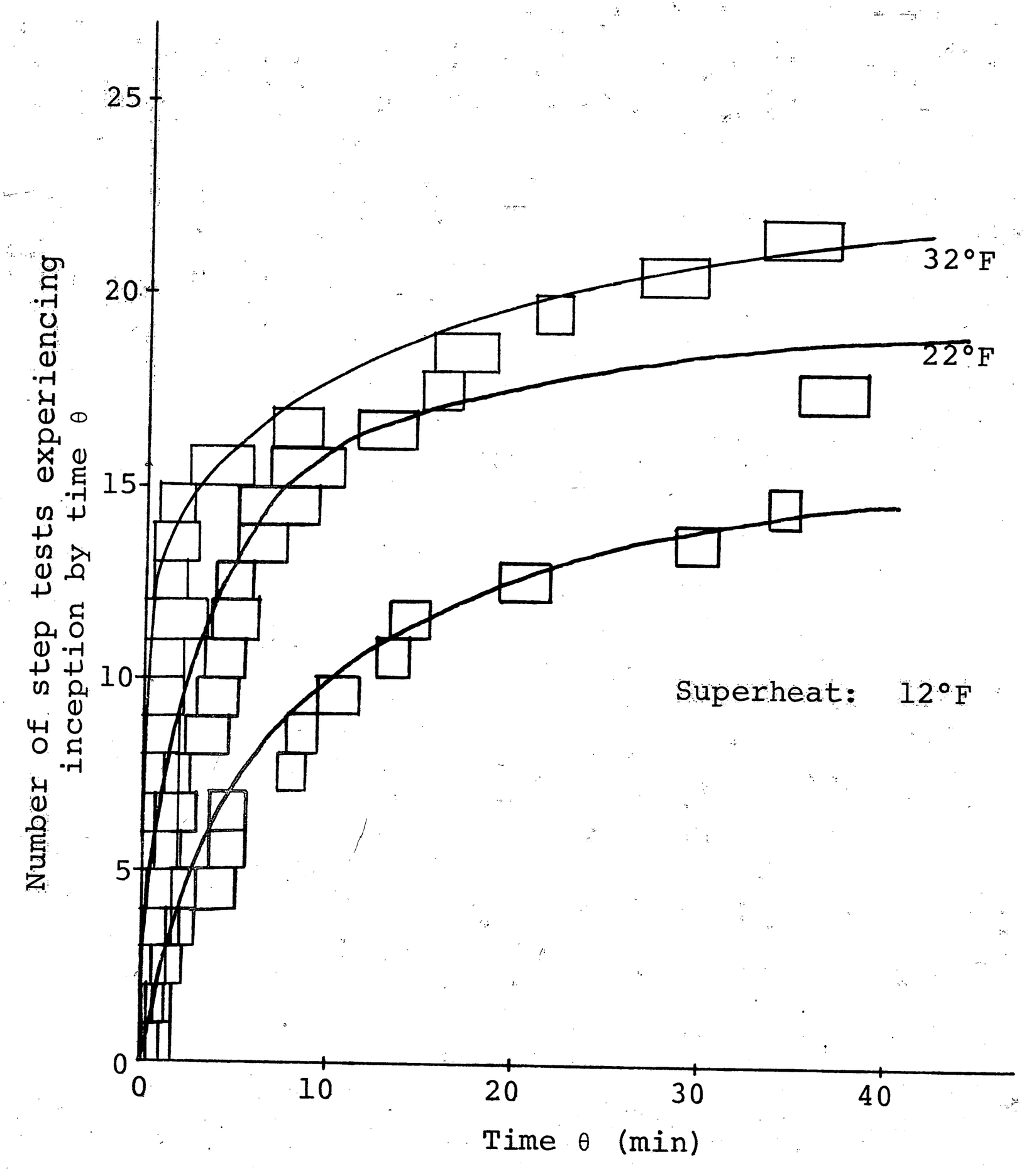

Figure 18. Step test results as accumulated probabilities.

been evaluated from Figure 19 and are given in Figures 20, 21 and 22. The cumulative curves for non-inception are straightforward; but the probability distribution curves need some explanation.

The probability distribution curve for each superheat step was found by measuring the slope of the corresponding cumulative probability curve. In the region of time 0-1 minute the dotted line of constant slope was differentiated; and thus, a constant probability of inception was graphed in Figure 21 for that time interval. Figure 22 is merely an enlargement of Figure 21 for time greater than one minute and has been included to clearly indicate the curve pattern.

Predictions of Most Probable Superheats

Before proceeding to predictions of probable superheat, it is necessary to realize that a temperature ramp may be approximated by steps of temperature using different methods. Figure 23 indicates four used by the author to synthesize probability distributions for ramps from the available step results. These synthesized probability curves, as well as a mean for results using methods 1 and 2, are given in Figures 24, 25, and 26. Each temperature ramp under consideration is represented by a separate figure. To clear up misgivings about how these

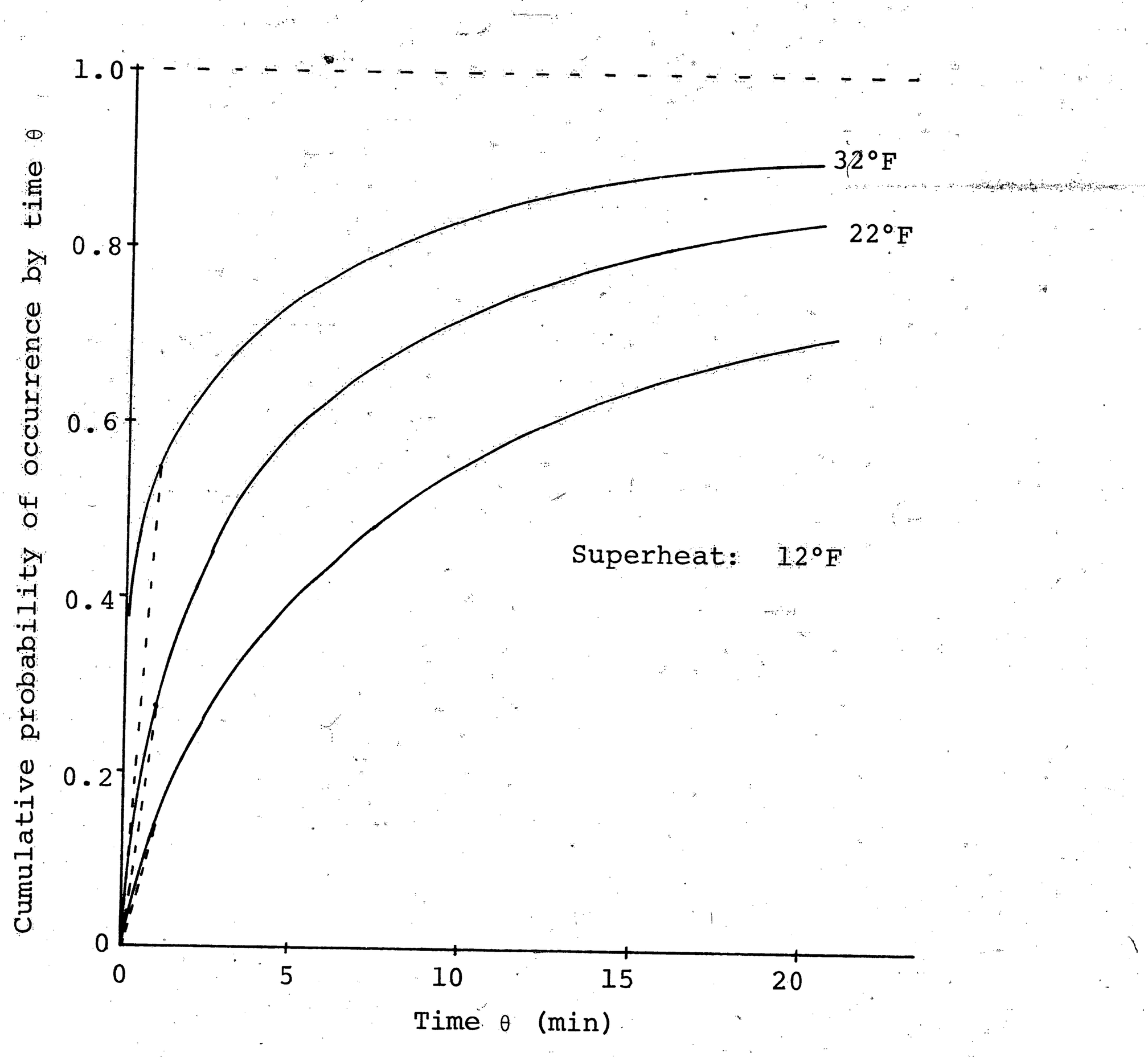

Figure 19. Normalized step test results indicating cumulative probability of occurrence.

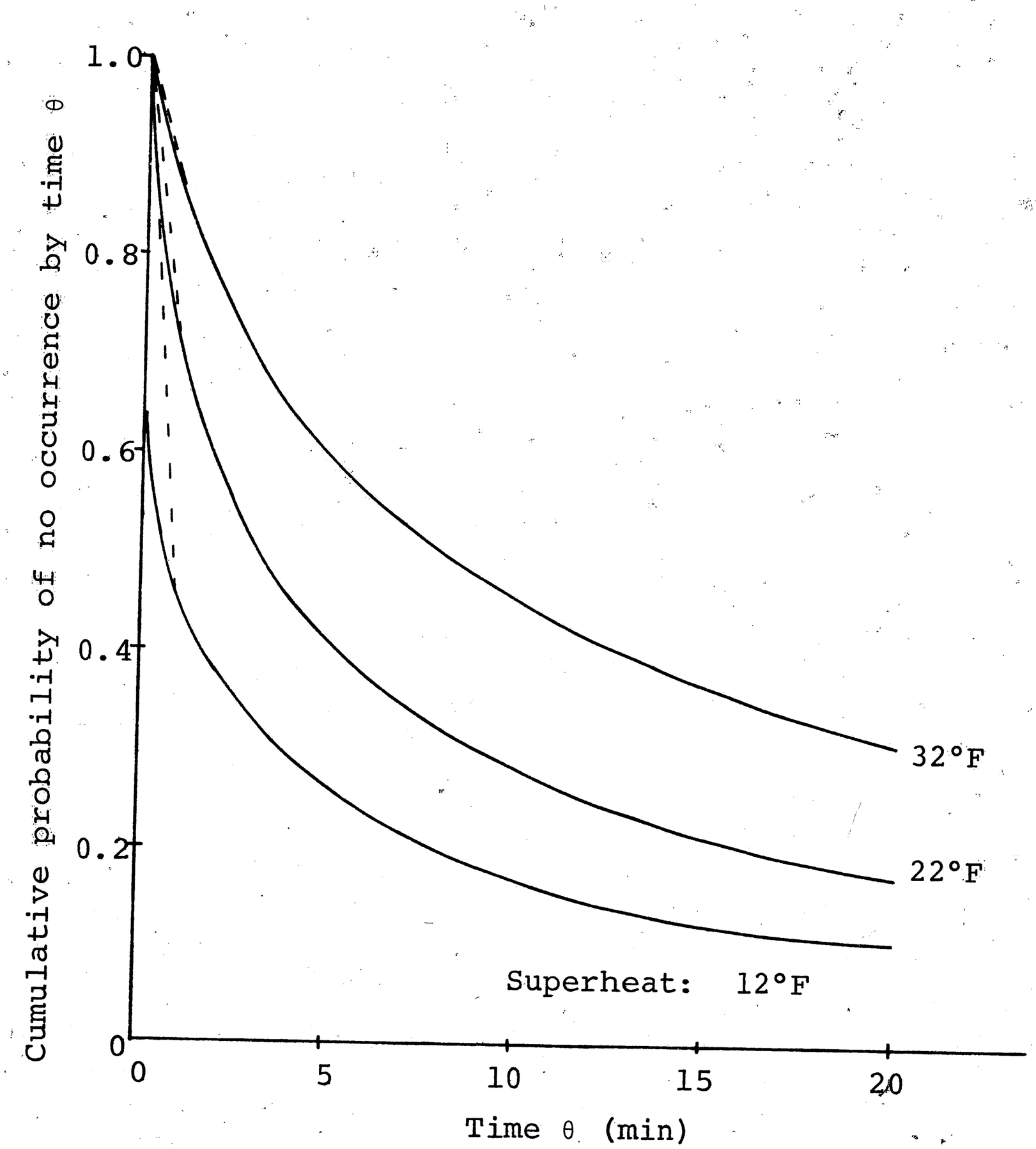

Figure 20. Normalized step test results indicating cumulative probability of non-occurrence.

Figure 21. Probability distributions for occurrence derived from step test results.

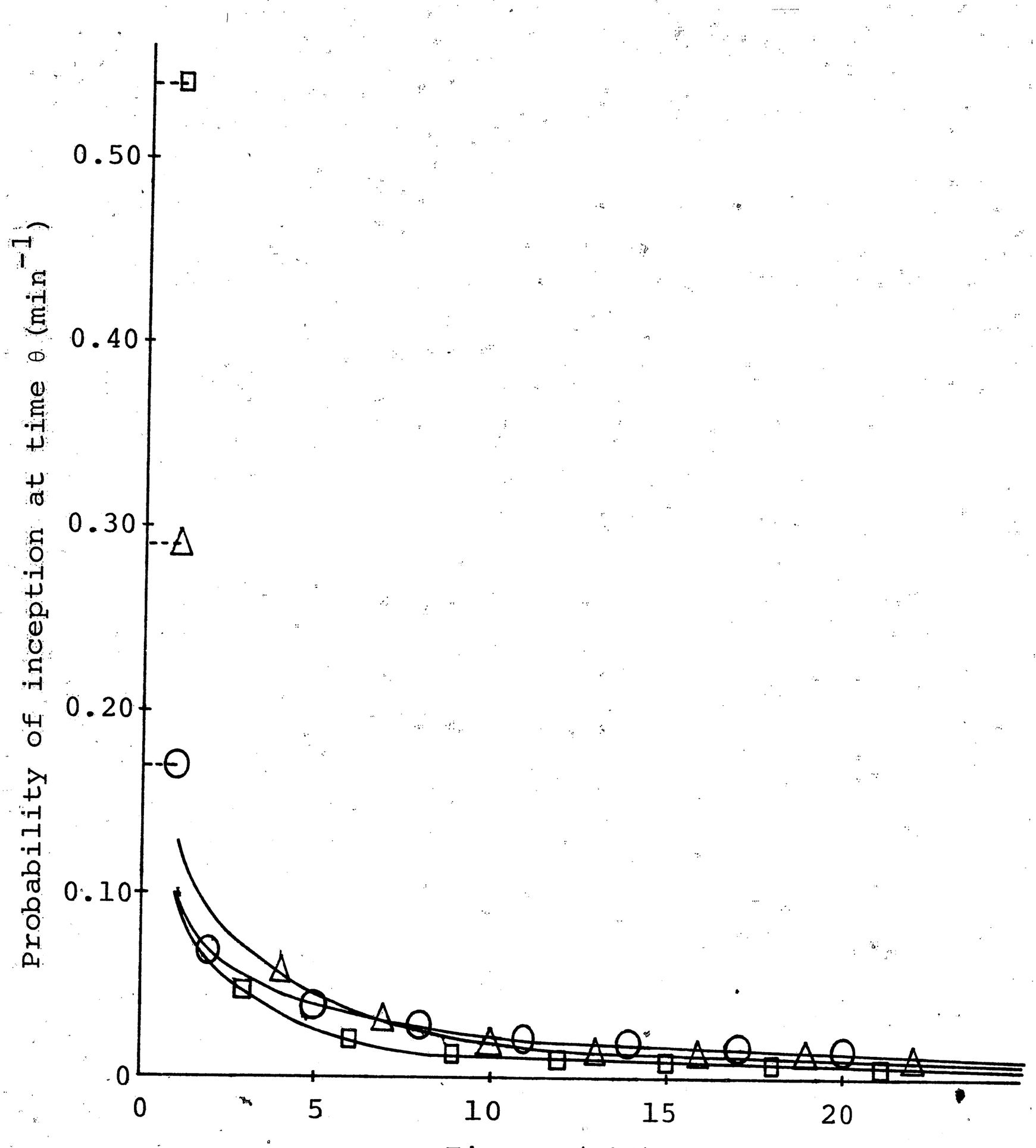

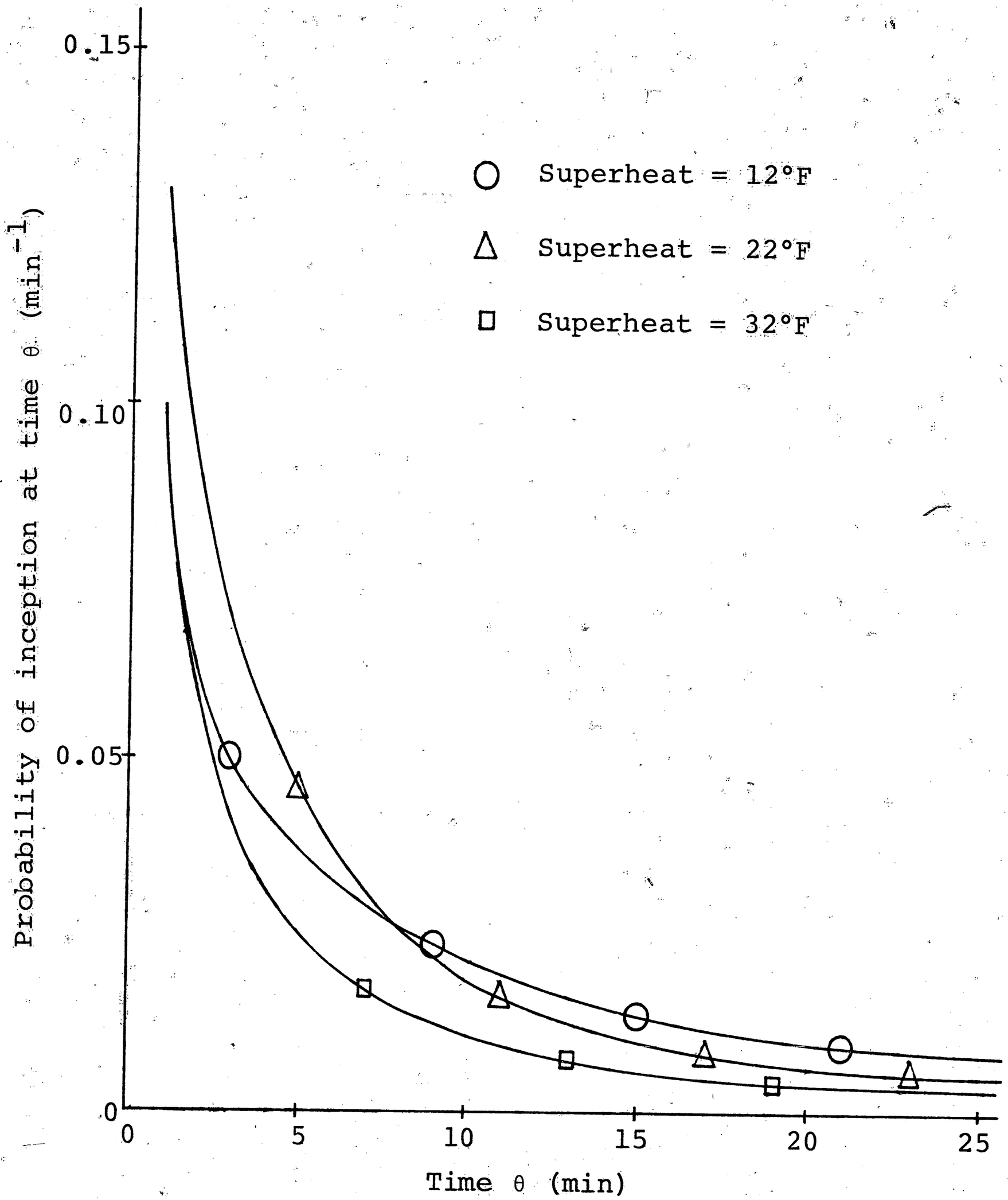

Figure 22. Enlarged portion of probability distributions.

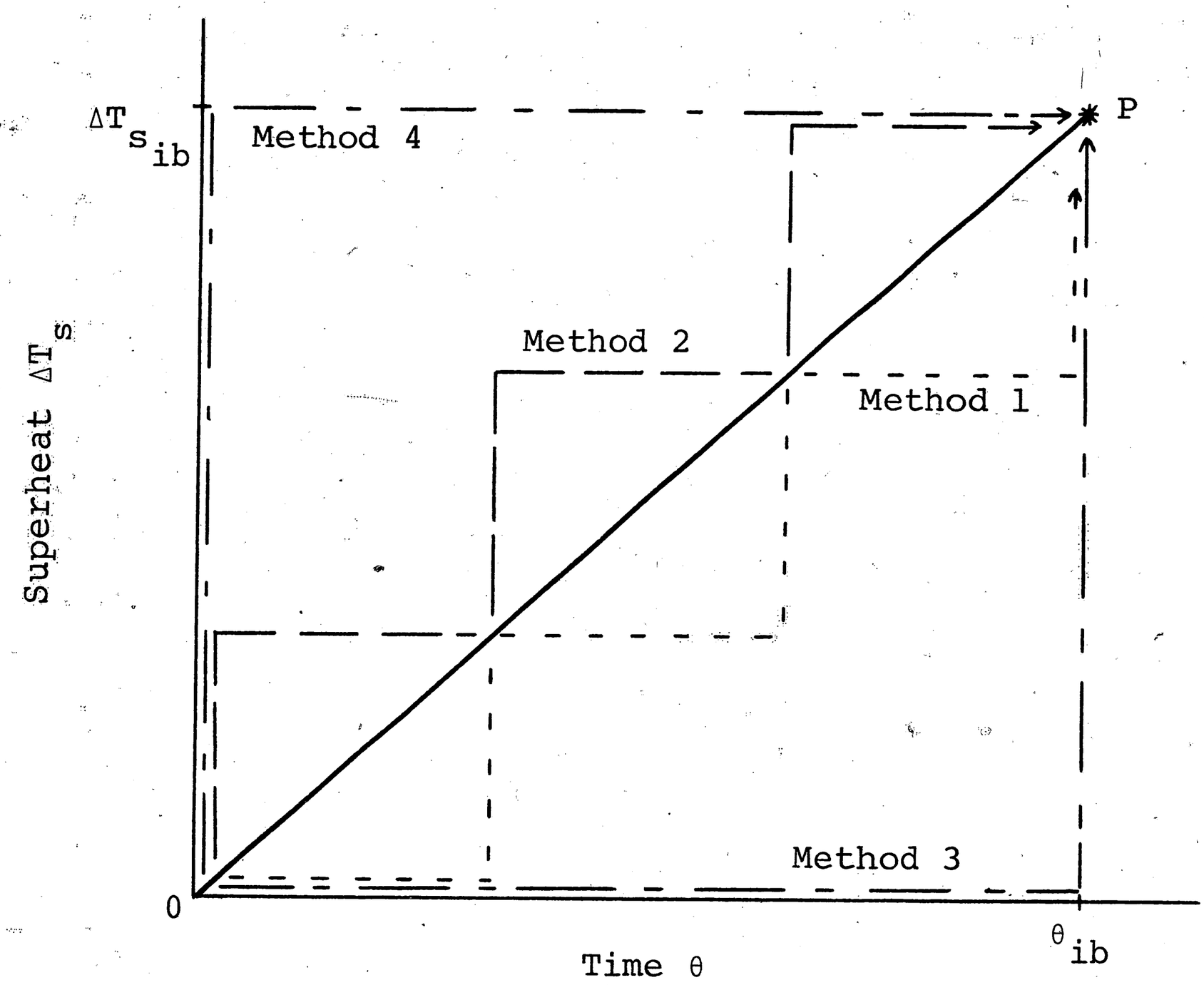

Figure 23. Methods of approximating a ramp by using steps of temperature.

Figure 24. Probability distributions for 2-3/4°F/min ramp synthesized from step test results.

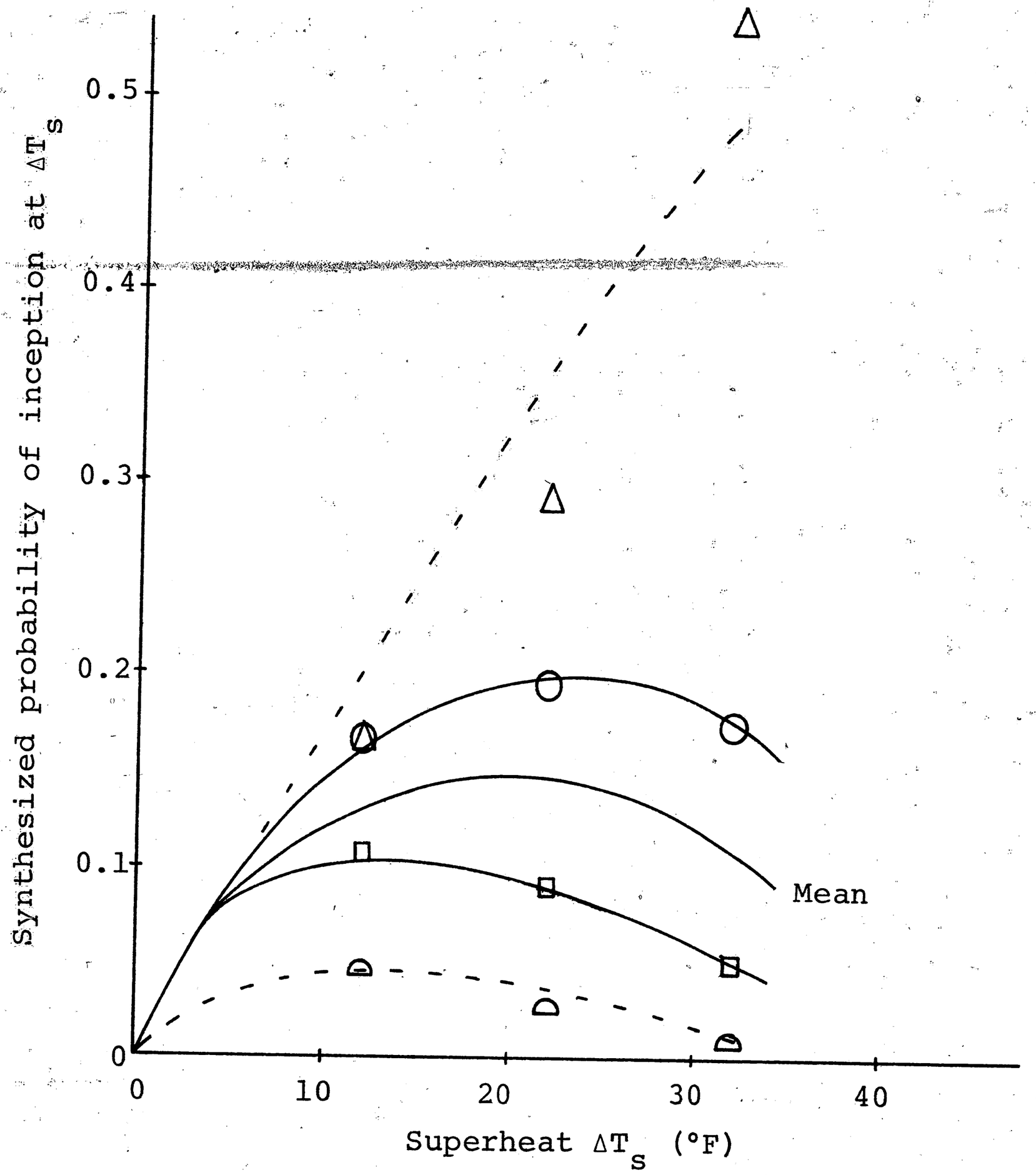

Key

○ Method 1

□ Method 2

△ Method 3

⌓ Method 4

Figure 25. Probability distributions for 5°F/min ramp synthesized from step test results.

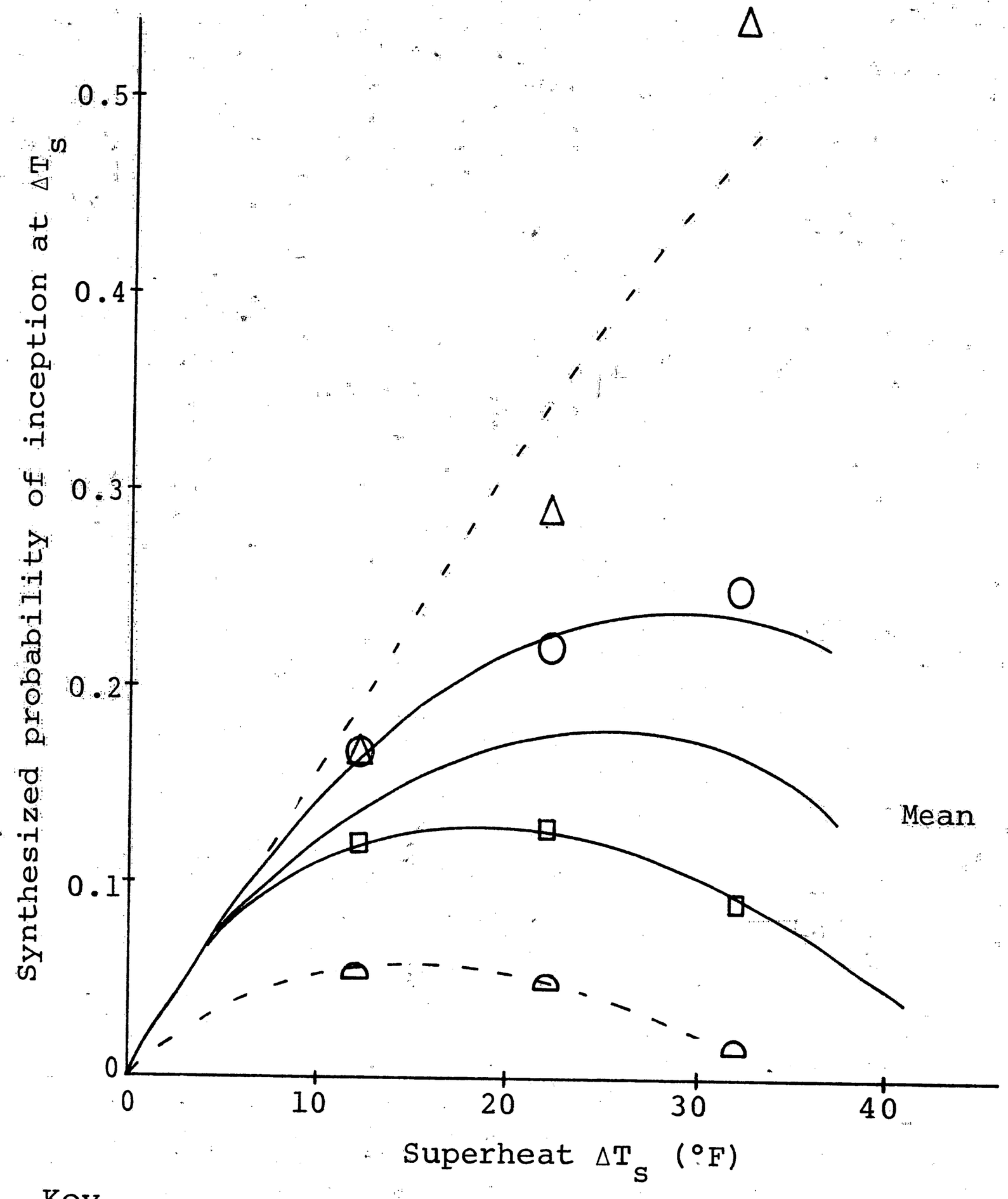

Figure 26. Probability distributions for 9-1/2°F/min ramp synthesized from step test results.

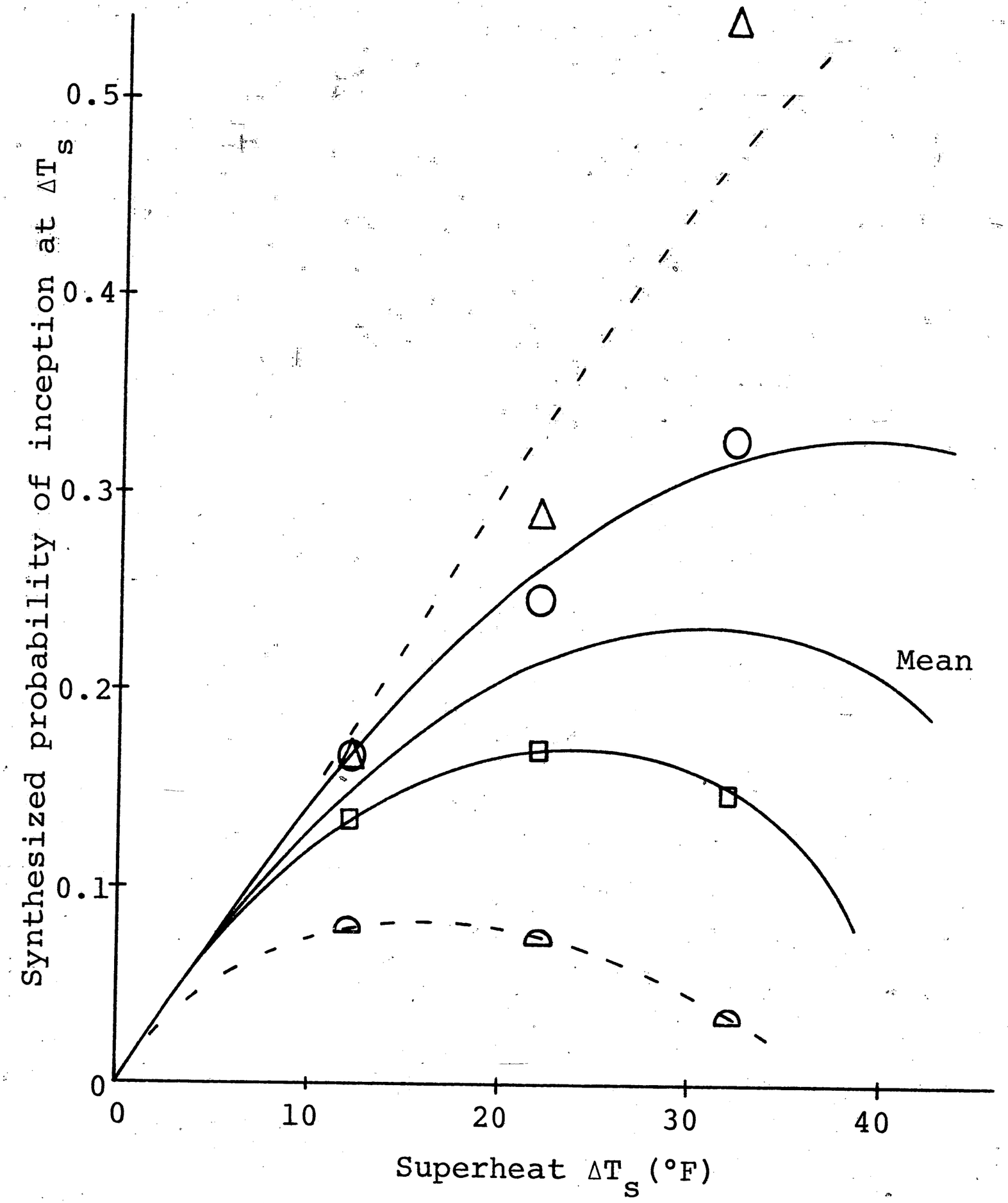

results were arrived at, two example points are described in detail below.

Example

Temperature Ramp: 9-1/2°F/min

Superheat at Inception: 32°F

ΔT_{S3} = 32°F $\theta_3 = \Delta T_{S3}/R$ = 3.37 min

ΔT_{S2} = 22°F θ_2 = 2.32 min

ΔT_{S1} = 12°F θ_1 = 1.26 min

Method 1 Approximation:

The synthesized probability of inception at ΔT_S = 32°F for R = 9-1/2°F/min using method 1 is given by the product of the probability of no inception during the interval $\theta_1 - 0$ = 1.26 minutes at zero superheat, the probability of no inception during the interval $\theta_2 - \theta_1$ = 1.06 minutes at 12°F superheat, the probability of no inception during the interval $\theta_3 - \theta_2$ = 1.05 minutes at 22°F superheat, and the probability of inception as time approaches zero at 32°F superheat. The values for the first three are taken from Figure 20 and are 1.0, 0.84, and 0.72, respectively. The fourth value is given by Figure 21 as 0.54. Thus the synthesized probability of inception is (1.0)(0.84)(0.72)(0.54) = 0.326.

Method 2 Approximation:

The synthesized probability of inception at ΔT_S = 32°F for R = 9-1/2°F/min using method 2 is given by the product of the probability of no inception during the interval $\theta_1 - 0$ = 1.26 minutes at 12°F superheat, the probability of no inception during the interval $\theta_2 - \theta_1$ = 1.06 minutes at 22°F superheat, the probability of no inception during the interval $\theta_3 - \theta_2$ = 1.05 minutes at 32°F superheat, and the probability of inception as time approaches zero at 32°F superheat. The values for the first three probabilities are given by Figure 20 as 0.82, 0.72, and 0.46, respectively. The fourth value is taken from Figure 21 as 0.54. Thus the synthesized probability of inception is (0.82)(0.72)(0.46)(0.54) = 0.147.

It is important to note at this time that these "synthesized" probability distributions are just that. The area under the curve is not equal to one as is the area under a true probability distribution curve. In this form they are of little value since they can not be compared to true probability distributions. To alleviate the problem the "mean" synthesized curve for each temperature ramp was normalized with respect to its area to yield a true probability distribution curve. These curves are plotted in Figure 27.

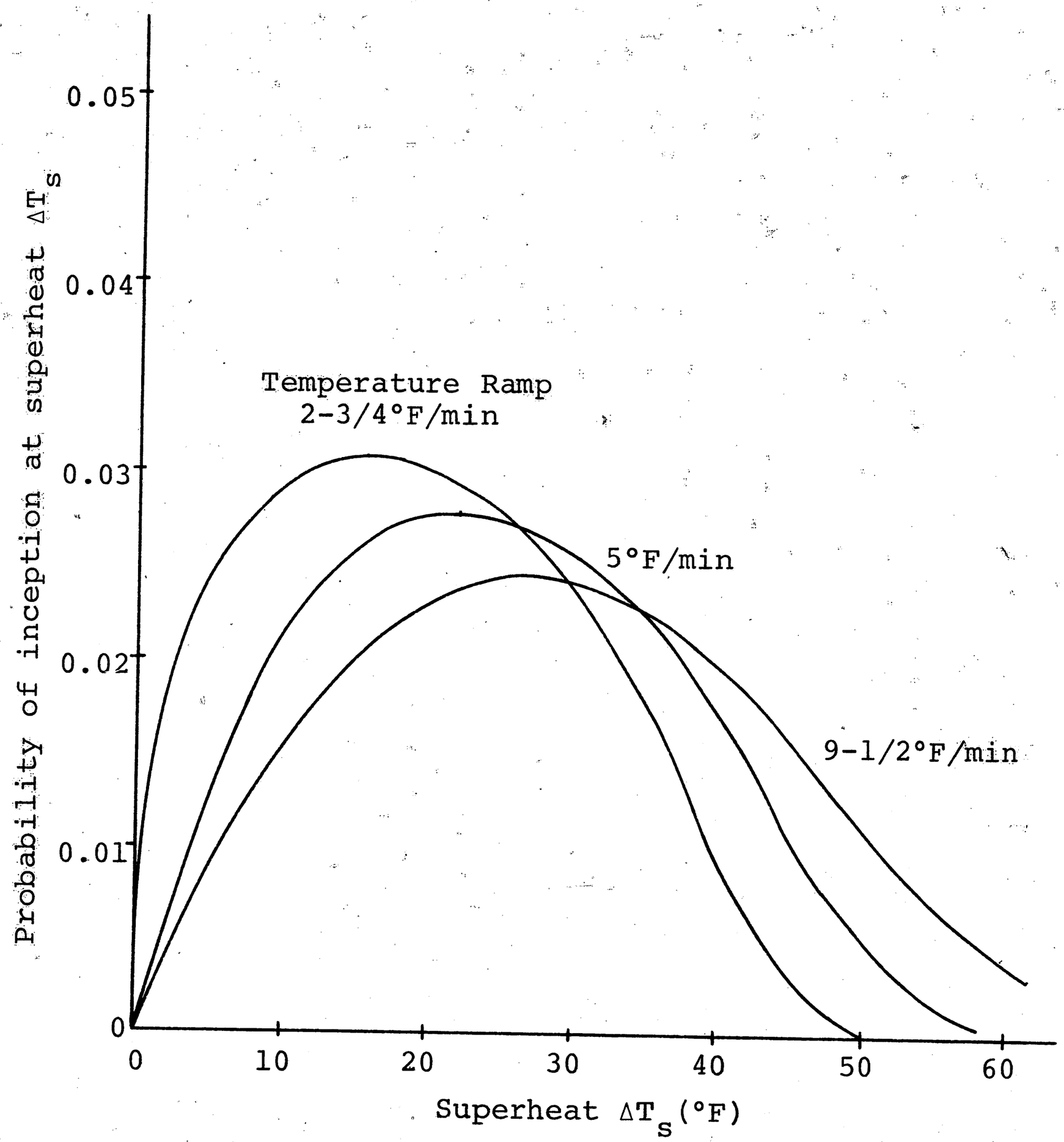

Figure 27. Normalized probability distributions derived from step test results.

Comparison of Experimental and Theoretical Findings

Two comparisons can now be made between the experimentally determined constant temperature ramp results and the predictions based upon experimental results for constant temperature step tests. The first relates to the agreement in the probability distribution curves arrived at by derivation and by direct testing. Figure 28 shows a typical set of curves--those pertaining to a temperature ramp of 5°F/min. Qualitatively, the curves have the same general nature; although the experimental curve seems more extreme in its tendencies, while the derived curve is flatter and more gentle by nature. This is readily explained by the limitations imposed on the model by the lack of step test data for many temperature steps: a maximum of three steps could be used in the approximation. Also, the derived curve shown is a mean of two approximating methods, and such a mean tends to damp out extremes demonstrated by either method in favor of a less varying average.

Quantitatively, the derived curve shows a lower maximum than the experimental curve. But this is also explained by the nature of the two curves. Since the area under each must be the same, a flatter curve would necessarily have a lower maximum than a curve which exhibits extremes.

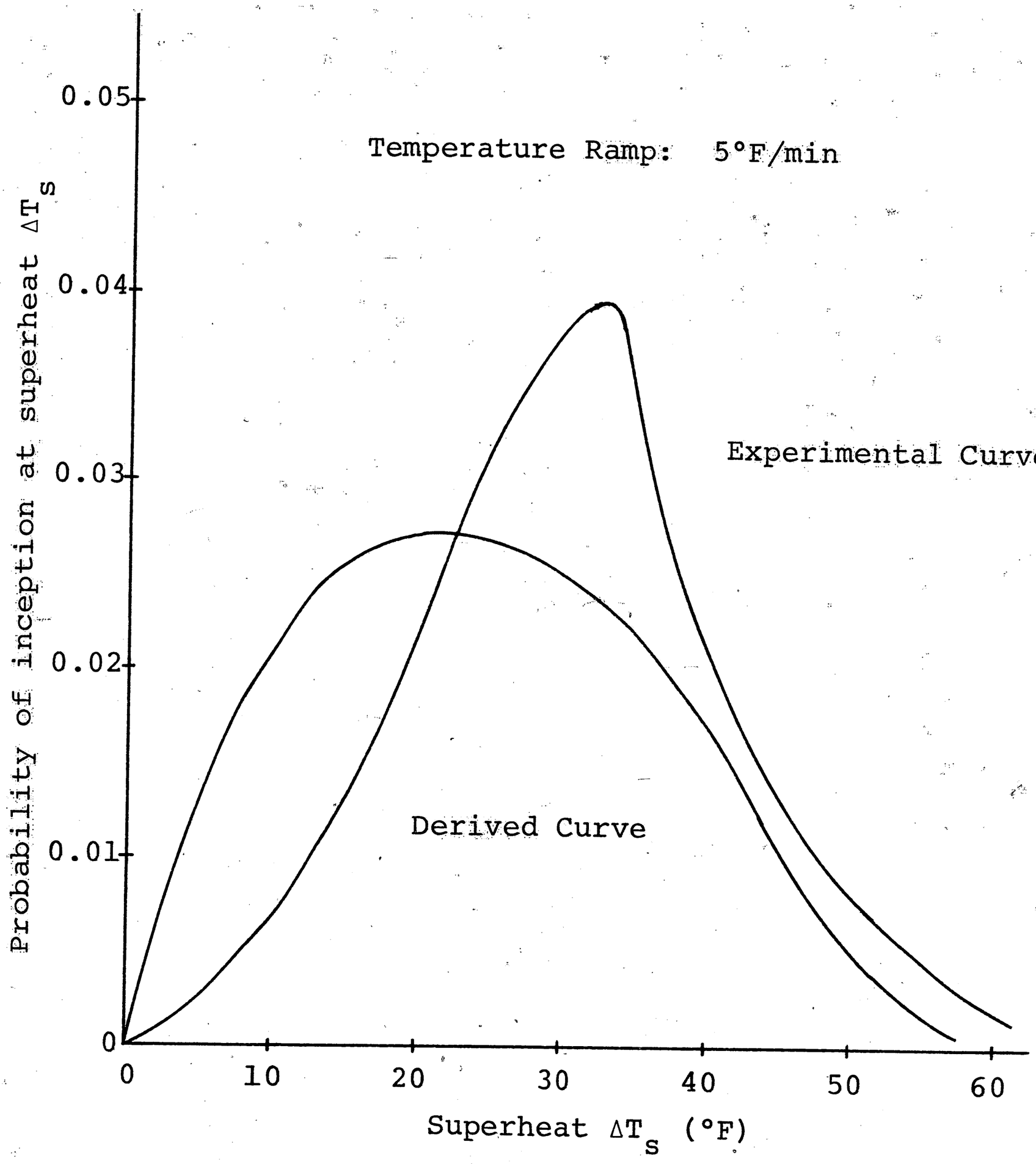

Figure 28. Comparison of probability distribution resulting from experimental ramp tests and derived from step tests.

The second comparison which can be made between the derived results and the experimental results involves the most probable superheat as a function of temperature ramp. Figure 16 indicated values determined by testing, and Figure 29 superimposes on those values the range of most probable superheat as indicated by approximation methods 1 and 2 in the figures dealing with synthesized probability distributions.

Qualitatively, the derived range imitates the experimental results fairly accurately. As anticipated the most probable superheat at inception increases by decreasing amounts as temperature ramp increases. Quantitatively, there is still a sizable error which would probably be substantially reduced if more and better step data had been available for analysis.

SUMMARY TO PART I

It has been shown that a statistical analysis of tests involving a uniform step of superheat may be used to predict the characteristics of a uniform ramp increase of temperature--notably the most probable superheat at which inception will occur for a given temperature ramp.

The mathematical model has intentionally been left simple. The temperature ramp of interest is approximated

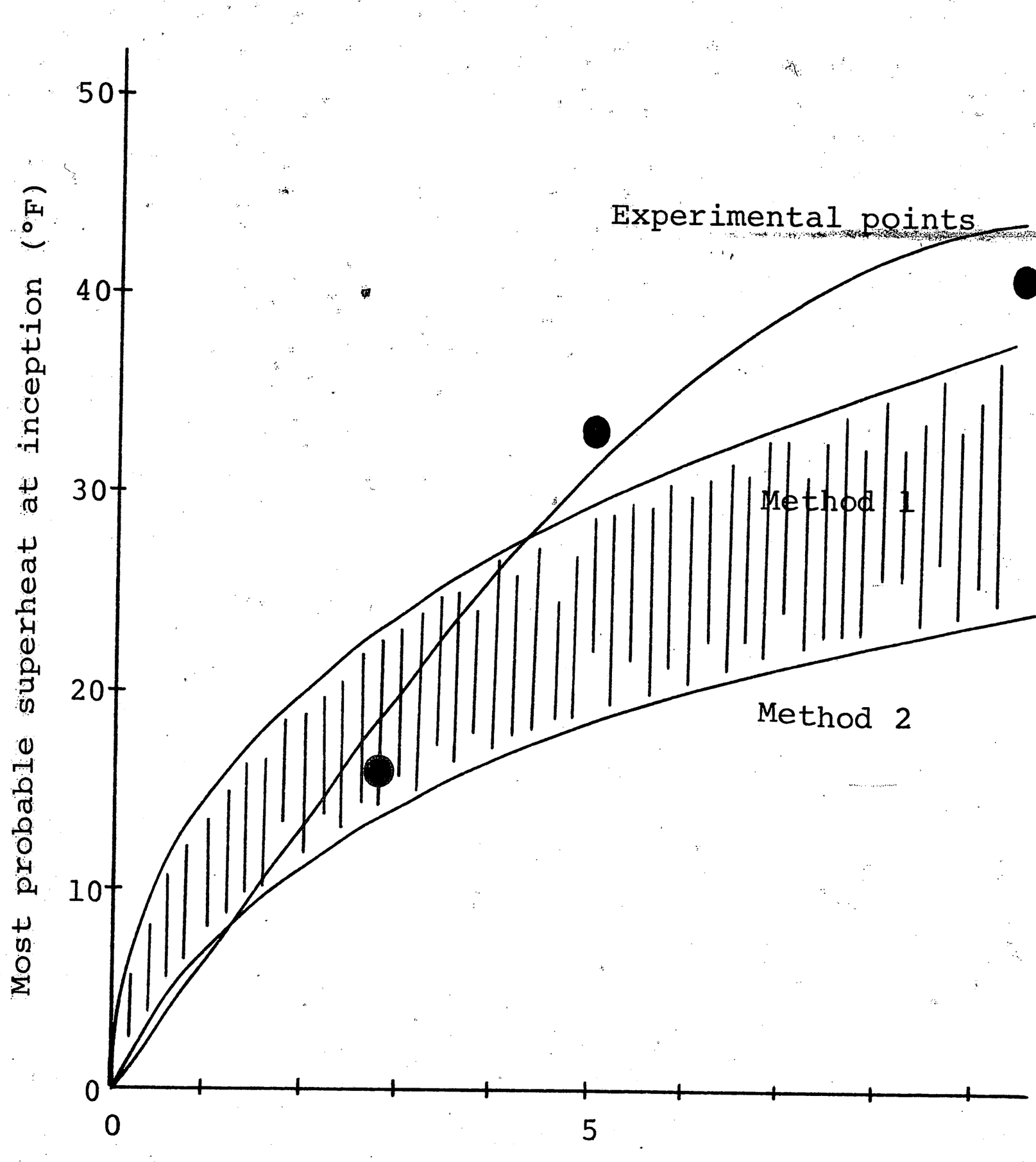

Figure 29. Comparison of most probable superheats resulting from experimental ramp tests and derived from step tests.

by a series of steps. If the cumulative probability distribution is known for each of the steps, other information may be derived; and a probability distribution for inception may be arrived at by properly combining this information. From the probability distribution it is easy to determine the most probable superheat at inception for the particular ramp. The importance of this method is its ease of use and adaptability. Once a large quantity of step data is available, any temperature ramp may be quickly modeled and its characteristics predicted.

The experimental work in support of the model has been of a gross nature and could not conceivably have rendered close quantitative results (although the maximum error amounted only to about 25%). Instead the value of the data is found in the qualitative comparisons, which indicate that a statistical model is a legitimate method of prediction. In particular, the nature of the probability distribution for inception is predicted to show higher peaks at lower superheats as temperature ramp decreases. Also, the most probable superheat at inception is seen to increase by decreasing amounts as ramp increases. Both of these predictions have been born out by the experiments.

It is now important that the experimental effort be continued using more sophisticated methods and

apparatus. Relative frequency approaches probability only when the number of tests is sufficiently large enough that the frequency tends to stabilize. Therefore, it is necessary to gather large quantities of data, which can be reliably used to predict quantitative results.

However, as was noted in the introduction of this section, it was the author's intention at this time merely to discover whether the foundations of the theory did in fact reasonably bear out what was found by experimentation. In this respect the work has been wholly successful.

TERMINOLOGY - PART I

English Letter Notation

a, b	probabilities defined when used
E	occurrence of event
$\bar{E}$	failure of event to occur
m	number of occurrences of a specified event
N	number of possible events for a specified experiment
p(E)	probability of occurrence of E
R	temperature ramp or increase in temperature per unit time
R(E)	relative frequency of E
T	temperature
T_{dg}	degassing temperature
T_{ib}	temperature at incipient boiling
T_{sat}	saturation temperature
T_w	measured wall temperature
T_{wi}	inside wall temperature
T_{wo}	outside wall temperature
ΔT_s	superheat ($T-T_{sat}$)
$\Delta T_{s_{ib}}$	superheat at incipient boiling

Greek Letter Notation

Δ	increment of change in superheat
δ	increment of time cooresponding to a specified superheat

Greek Letter Notation (continued)

θ	time
θ_{ib}	time at incipient boiling

PART II

INCEPTION OF "BOILING" IN A FLOWING SUPERHEATED LIQUID

INTRODUCTION TO PART II

In studies of flowing superheated liquids a notable characteristic is that the maximum superheat which is achieved by the liquid tends to decrease as Reynolds number increases. Several theories involving turbulent fluctuations of pressure and velocity have been advanced to explain this tendency. An alternative based upon cavitation in vortex cores formed by flow over obstructions such as thermocouple housings or pressure taps is presented in the following section. Included in the discussion are brief descriptions of the cavitation phenomenon and the parameters which influence it; the wake characteristics in a flow over a bluff body; and a two-dimensional free vortex model.

The trend in question is explained in terms of a local pressure differential which remains constant regardless of Reynolds number and which is supported by liquid potassium test data received from John C. Chen, formally

of Brookhaven National Laboratory. Also, Bernoulli's equation is reduced to demonstrate that a significant pressure drop may be found across a vortex; and that it is indeed possible that inception occurs in these cores of low pressure.

THE PHENOMENON OF CAVITATION

Definition

When a body of liquid is heated under constant pressure or when its pressure is reduced at constant temperature, a state is ultimately reached at which vapor-filled bubbles or cavities become visible and grow. This condition is known as boiling if caused by temperature rise, and cavitation if caused by dynamic pressure reduction at essentially constant temperature. The classification of cavitation types includes cavitation in a flowing stream, on moving bodies, and without major flow (vibratory cavitation). Development stages are broken roughly into incipient--limited zone of cavitation and small bubbles--and developed, where increased vaporization occurs. Our primary concern involves incipient cavitation in a flowing stream, although incipient and developed stages are sometimes indistinguishable in superheated liquids as will be explained later.

Variables that affect inception and the subsequent character of cavitation in flowing liquids are many. Important ones include boundary geometry, flow variables and the critical pressure at which a bubble can be formed or a cavity maintained. Other variables include fluid properties, contaminants, and surface conditions. It has become general practice to use a basic parameter to predict cavitation and to indicate the effects of lesser variables as deviations from those predictions.

Cavitation Number

To develop the basic parameter, a relative flow between an immersed object and the surrounding liquid is considered. A variation in pressure along the object surface results, and the difference between the pressure at a point on the object and the pressure in the free stream is proportional to the square of the relative velocity. If Reynolds number effects are neglected, this proportionality will depend only on the shape of the object in the absence of cavitation. By increasing the relative velocity for a fixed value of free stream pressure or by lowering pressure with velocity held constant, the absolute values of all the local pressures on the surface of the object will decrease. If surface tension is ignored, the pressure of the contents of a bubble formed in this region will be the same as the local pressure.

The cavitation number, K, is defined as

$$K \equiv \frac{P_\infty - P_b}{\frac{1}{2}\rho V_\infty^2} \qquad (1)$$

where P_∞ = absolute free stream static pressure

P_b = absolute static pressure in cavity

ρ = liquid density

V_∞ = free stream velocity

In general the cavitation parameter may be viewed as the ratio of the pressure available to collapse the cavity to the pressure available for inducing formation or growth of the cavity. An additional simplification can be made if it is assumed that cavitation occurs when normal stresses at a point in the liquid are reduced to zero. In this case the bubble pressure will be equal to the vapor pressure, and

$$K = \frac{P_\infty - P_v}{\frac{1}{2}\rho V_\infty^2} \qquad (2)$$

where P_v = static vapor pressure.

Scaling and Scale Effects

Scaling is the extrapolation of cavitation behavior from one set of conditions to another. Scale effects are deviations from the elementary definition of

the cavitation number for the same event (e.g., inception). The general scale effects problem may be classified into three headings:

1) The critical pressure at the location of inception may not be equal to the vapor pressure.
2) The minimum pressure in the flow field may not be constantly related to the dynamic pressure.
3) Turbulence and vorticity may cause the location of the minimum pressure to be away from a boundary and therefore, the pressure may differ greatly from the body surface value.

Deviations of the first category are directly related to the nature and source of nucleii and the related bubble dynamics. Surface tension and viscosity are recognized factors of influence in these concepts. The second category encompasses the general Reynolds scaling problem and will not be discussed.

The third category concerns concepts of boundary wall pressure, time scale effects, boundary layer turbulence, and pressure minima in the boundary layer. At high Reynolds numbers the shear layers in wakes are turbulent. A feature inherent to all turbulent flows is the unsteady variation of pressure with peaks well below the static level. The intensity of these fluctuations appears to be directly related to the mean shear in the

flow. Because of these turbulent fluctuations in pressure, cavitation is often observed to occur at values of mean pressure at the boundary surface which are well above the vapor pressure. The mechanism described in this work, however, is not based on such pressure fluctuations since it is felt that a relatively long-lasting low pressure vortex core is a much more acceptable location for inception.

Influence of Fluid Properties

Several fluid properties influence cavitation inception and development. Surface tension always works to close a cavity that is open is a fluid. It is conceivable that in a flowing system with a short low pressure zone, a liquid with high surface tension forces would not experience cavitation, whereas a liquid with low forces would tend to cavitate. Assuming no gas or contaminant presence, equilibrium theory indicates that

$$P_v = P_L + \frac{2\sigma}{R} \tag{3}$$

where P_v = static pressure in the bubble

P_L = local static pressure in the liquid

σ = surface tension

R = bubble radius.

If the vapor pressure is greater than the combined forces

on the right of the equation, the bubble will grow. If it is less, the bubble will collapse.

The effect of viscosity is to produce a damping loss of mechanical energy during the growth and collapse processes. Consequently, it would be expected that increases in viscosity will decrease the maximum cavity size and the rates of growth and collapse. In short viscosity appears as an equivalent change in the internal cavity pressure. Poritsky [4] described the effects of viscosity and surface tension for an incompressible liquid by

$$P_v = P_L + \frac{2\sigma}{R} + 4\mu \frac{dR/dT}{R} \qquad (4)$$

where μ = shear coefficient of viscosity.

Viscous effects are highest in the growth and collapse processes where the velocity dR/dT may be large.

Thermodynamic properties such as latent heat of vaporization and specific heat of the liquid also affect cavitation by influencing the interchange of matter between liquid and vapor phases. Properties of various liquid metals and other fluids are given in Table 1.

Problems of Superheated Cavitation

At this point it is necessary to reveal some of

Table 1. Thermodynamic Properties of Various Liquids [10].

MATERIAL	WATER		MERCURY		SODIUM		POTASSIUM		LITHIUM		ETHANAL	GLYCERIN
PROPERTY	70°F	300°F	70°F	500°F	500°F	1500°F	500°F	1500°F	500°F	1500°F	68°F	68°F
Density, slugs/ft³	1.939	1.779	26.27	25.17	1.724	1.474	1.518	1.249	0.97	0.891	1.53	2.45
Specific weight, γ(lb/ft³)	62.43	57.3	845.9	810.3	55.50	47.45	48.88	40.20	31.21	28.35	49.3	78.8
Surface tension, σ(lb/ft) × 10²	0.5015	0.322	3.187	2.875	1.202	0.83	0.545	0.425	2.625	2.122	0.153	
Bulk modulus, (psi) × 10⁻⁶	0.31	0.248	4.11	3.94	0.765	....	....	....	0.160	0.140	....	0.630
Specific heat, Btu/(lbm-°F)	1.00	1.03	0.033	0.032	0.3155	0.3030	0.1864	0.1891	1.03	0.991	0.581 (77°F)	0.57
Thermal diffusivity, (ft²/sec) × 10⁵	0.147	0.186	4.694	7.03	71.4	63.6	73.1	62.8	19.44	21.42		
Heat of vaporization, Btu/lbm	1054	910	127.7	126.5	1970	....	932.0	812.4	2600.0	2600.0		
Vapor pressure, psia	0.36	67.62	2.5×10^{-5}	1.93	~10⁻⁵	7.737	<0.001	24.66	0.001	0.1	0.85	2×10^{-6}
Prandtl number (dimensionless)	6.8	1.18	0.026	0.0091	0.0065	0.0038	0.0047	0.0032	0.05	0.022	....	12.5
Kinematic viscosity, ν(ft²/sec) × 10⁶	10.8	2.17	1.174	0.75	4.6	2.34	3.46	2.15	10.8	6.17	16.4	12,700

the problems involved in attempting to describe the cavitation phenomenon as it pertains to superheated liquids. The simplest way to do this is to compare temperature and pressure relations of a superheated liquid to those of a normal liquid, such as water. Temperature-pressure curves are pictured in Figure 30. The most notable difference is the relative position of various pressures--local, free stream, and vapor. In a normal fluid the vapor pressure corresponding to the free stream temperature is less than the free stream pressure. In a superheated liquid the opposite is true. This important difference causes two problems to arise.

The first concerns the cavitation number. The definition of K given by equation (2) is

$$K = \frac{P_\infty - P_v}{\frac{1}{2}\rho V_\infty^2} \tag{5}$$

In the case of a superheated liquid, K is a negative number. Therefore, the limited results available for use in predicting cavitation are seen to be useless for predicting occurrence in superheated fluids. Also, it is questionable that this definition of K has any true meaning when used in reference to superheated liquids. Thus, it is necessary to refrain from using available cavitation data in this analysis. Instead, it is useful only to

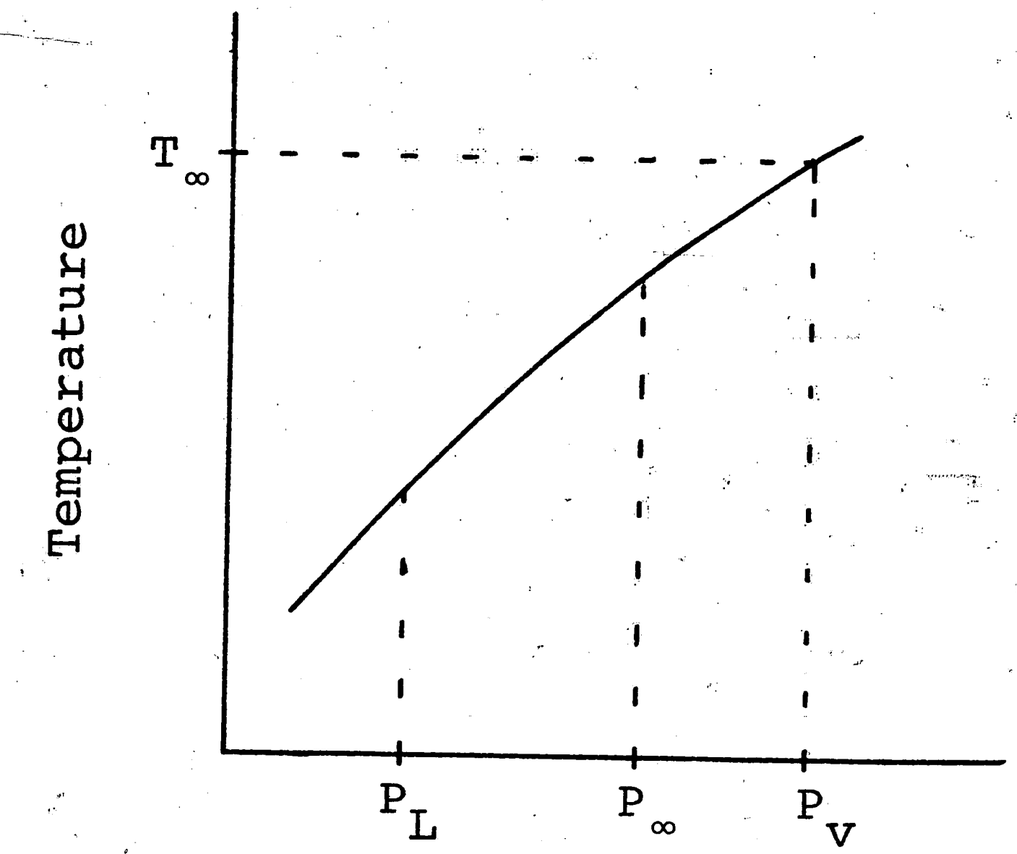

(a) superheated liquid

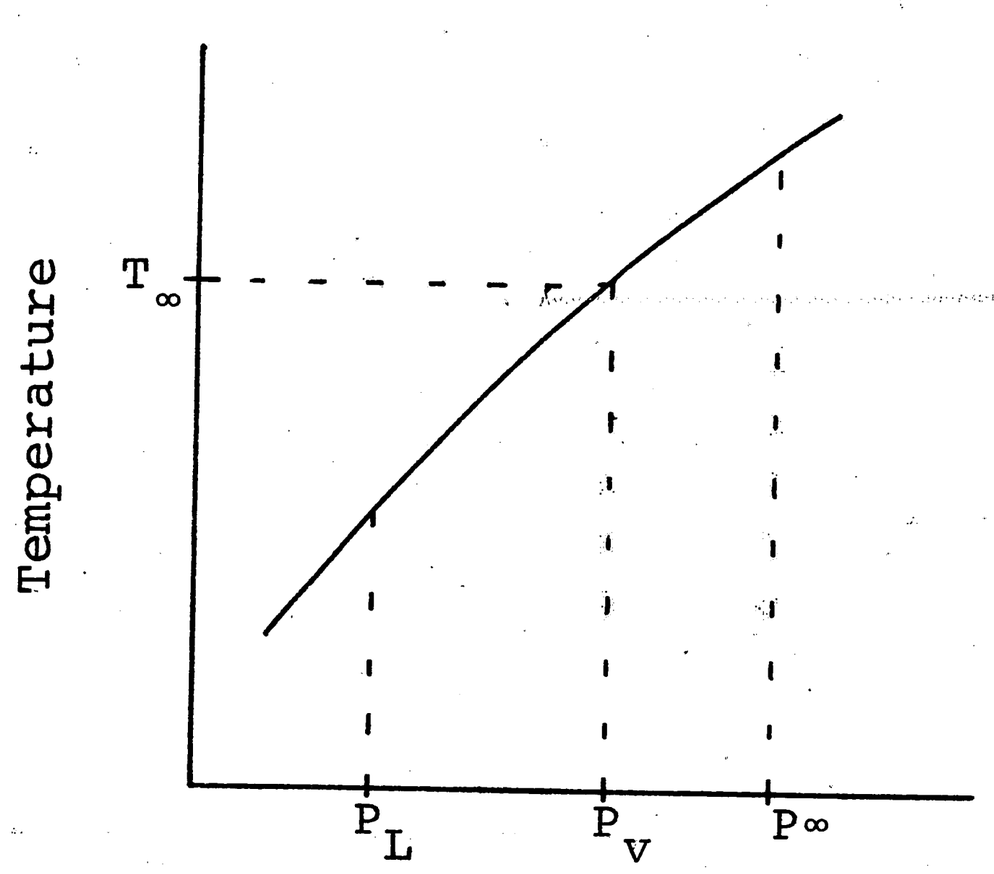

(b) normal liquid

Figure 30. Relative positions of pertinent pressures in superheated and normal liquids.

recognize the mechanism of the cavitation phenomenon and the parameters which influence it.

A second problem arises from the fact that in a superheated liquid there exists such a large driving potential that once a bubble is conceived, it grows rapidly to a large size. Therefore, it is difficult to divide incipient and developed cavitation into separate, defined stages since the two are very much intermingled.

LOCATION OF INCEPTION

Flow Past a Bluff Body

To determine where inception is likely to occur, we return to the flowing fluid system. Some knowledge of the flow patterns observed in incompressible flows past a bluff body in the form of a circular cylinder whose axis is perpendicular to the direction of the flow is of use to us. As the characteristic Reynolds number,

$$Re_D = \frac{\rho V_\infty D}{\mu} \qquad (6)$$

where D = diameter of cylinder,

increases, the nature of the wake and the boundary layer change progressively through a well defined sequence of metamorphoses.

At very low Reynolds number the viscous forces are much larger than the inertia forces, and the flow resembles the potential flow of a perfect fluid. In the range $0.1 < Re_D < 5$ the streamlines open out behind the obstacle and form a separated flow region. As Reynolds number increases to 30, two stationary vortices form symmetrically behind the cylinder. A separation surface, which represents a vortex layer, forms a boundary between the stream flow and the vortex pair. During further increases above 30 or so, the wake develops a periodic pattern known as the Kármán vortex street. This flow pattern is represented as vortices of alternating sign shed periodically on either side of the cylinder. Between Reynolds numbers of 40 and 150 regular vortex streets are formed and the wake flow is laminar. For $Re_D > 300$ the wake becomes fully turbulent and periodicities are harder to observe. Finally, in the range $10^5 < Re_D < 10^6$ the boundary layer itself becomes turbulent, flow separation is delayed, and the wake behind the body narrows markedly. Figures 31 and 32 show the transition of the wake and boundary layer for various values of Reynolds number.

Vortices in Wakes

In wakes zones of high shear stress develop between the fast-moving free stream fluid and the slow-

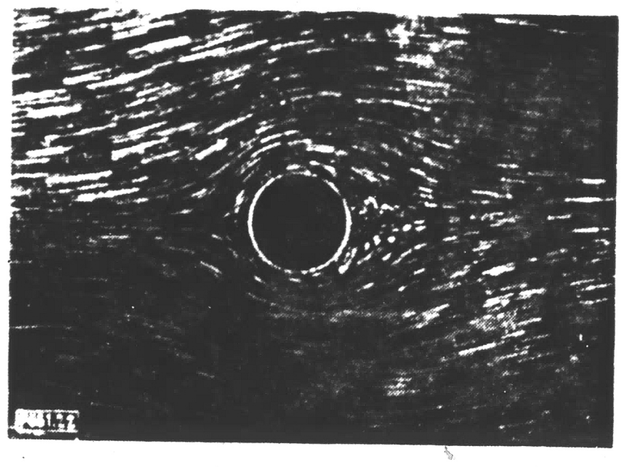

(a) Re_d = 3.9

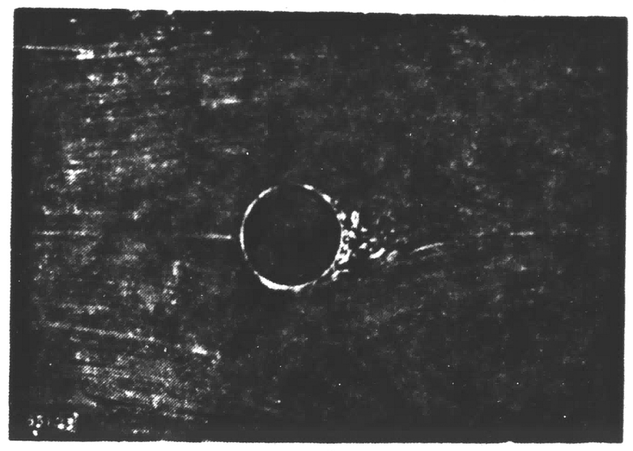

(b) Re_d = 18.6

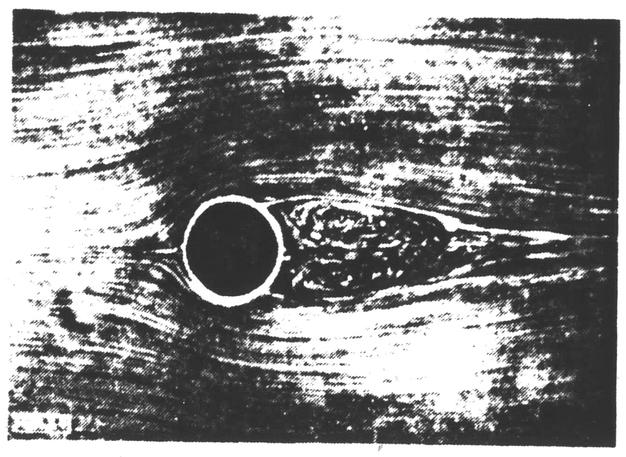

(c) Re_d = 33.5

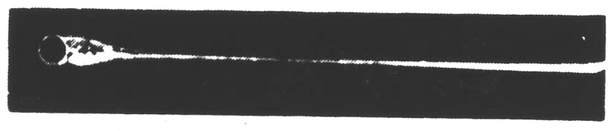

(d) Re_d = 31.6

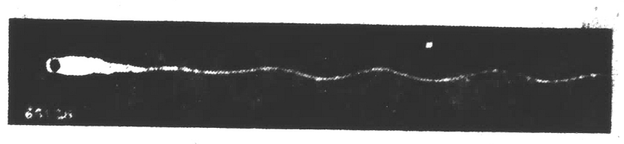

(e) Re_d = 54.8

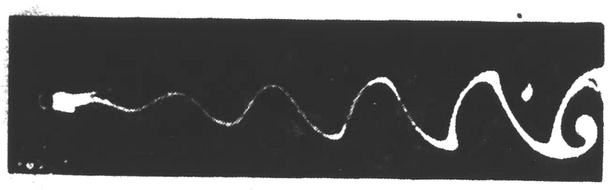

(f) Re_d = 65.2

(g) Re_d = 73

(h) Re_d = 101.5

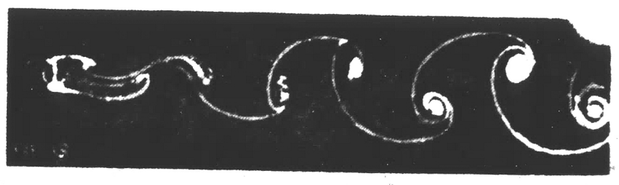

(i) Re_d = 161

Figure 31. Flow about a circular cylinder [8].

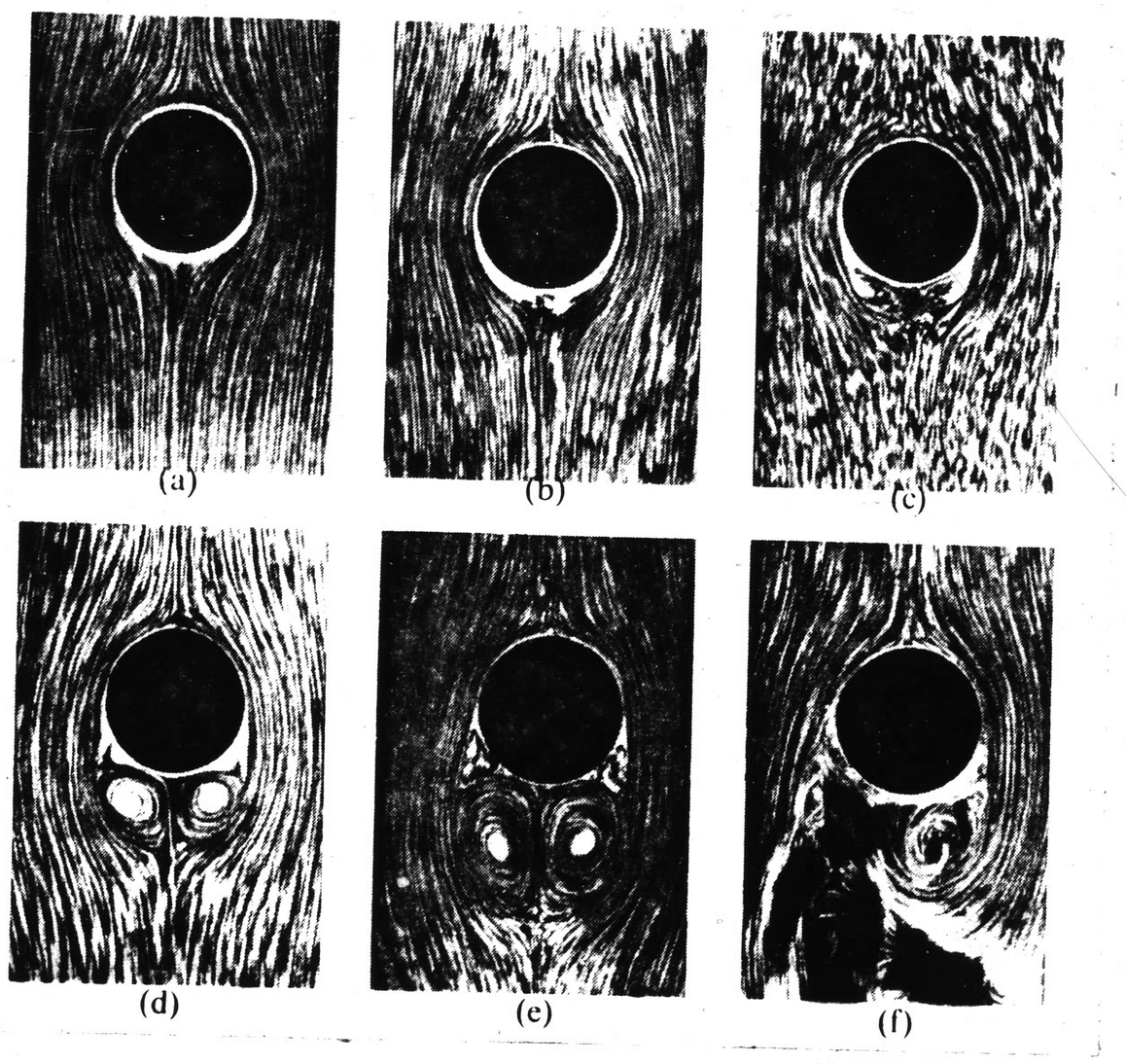

Figure 32. Development of vortices in flow past a circular cylinder. First photograph shows the start of fluid motion [8].

moving wake fluid. As a result, the boundary of a wake is a zone of high intensity eddying. When cavitation occurs in a wake it usually appears first in the centers of finite vortices found in the shear zone of the wake boundary. These are the centers of minimum pressure as opposed to the minimum pressure points along surfaces of more streamlined bodies.

Cavitation may appear as traveling or fixed in nature. Figures 33 and 34 show cavitation in the wake caused by boundary layer separation from a sphere. Here inception occurs not on or adjacent to the body, but on the surface of the separation zone. The cavitation is of the vortex type; but since the flow is very unsteady, the vortices are not regular, but are random and transient. Such vortex cavitation at separation zones of bluff bodies may also be the preliminary stage to the formation of a fixed cavity.

Cavitation will develop whenever there is a sufficiently high shear rate in a region to form vortices in which absolute pressure in the core drops to a critical pressure for the given flow conditions. The life of a vortex cavity may be very long as compared with that of traveling cavities, since once the vortex is formed, the angular momentum of the liquid in it prolongs the life of

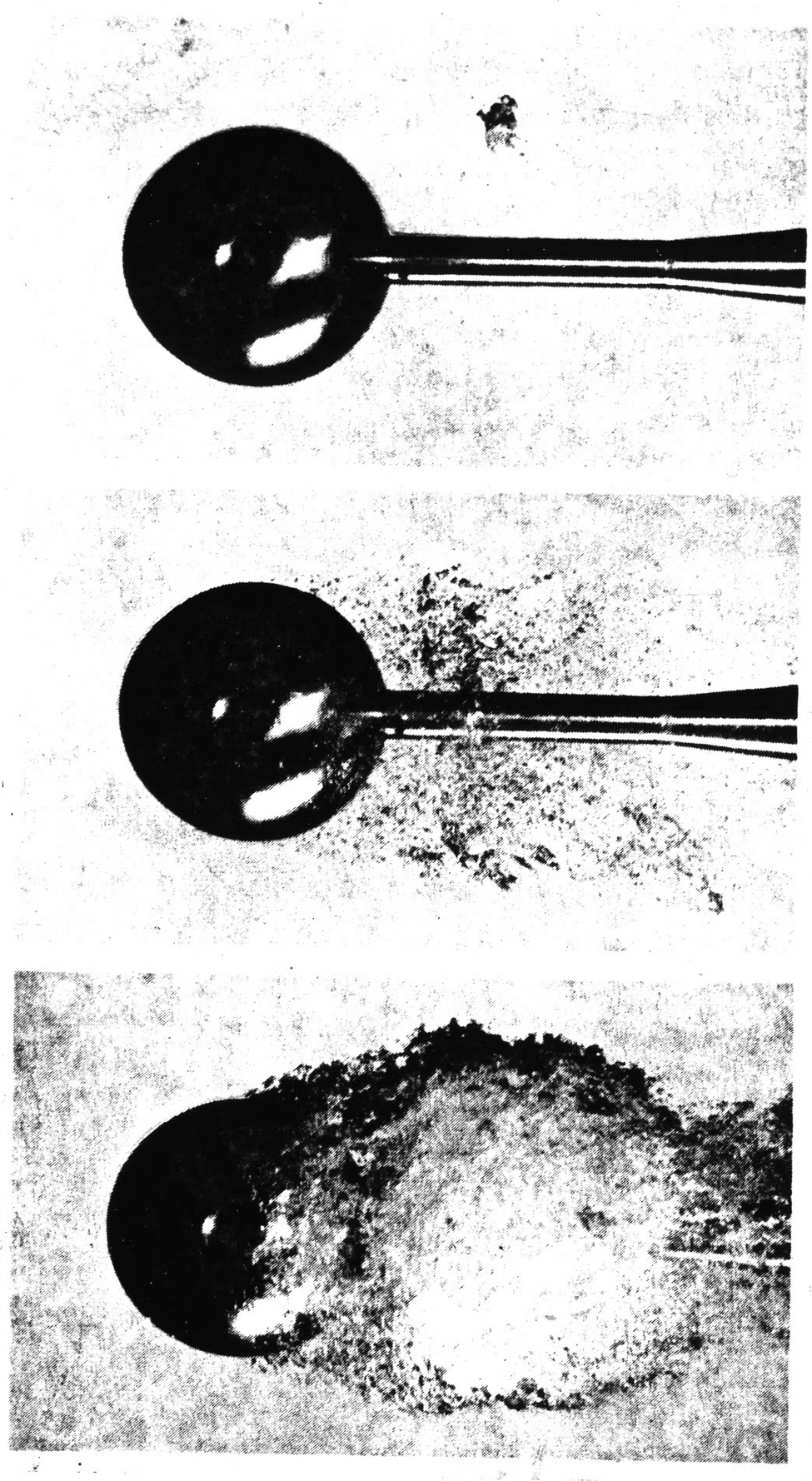

Figure 33. Cavitation in the wake of a sphere as velocity increases [7].

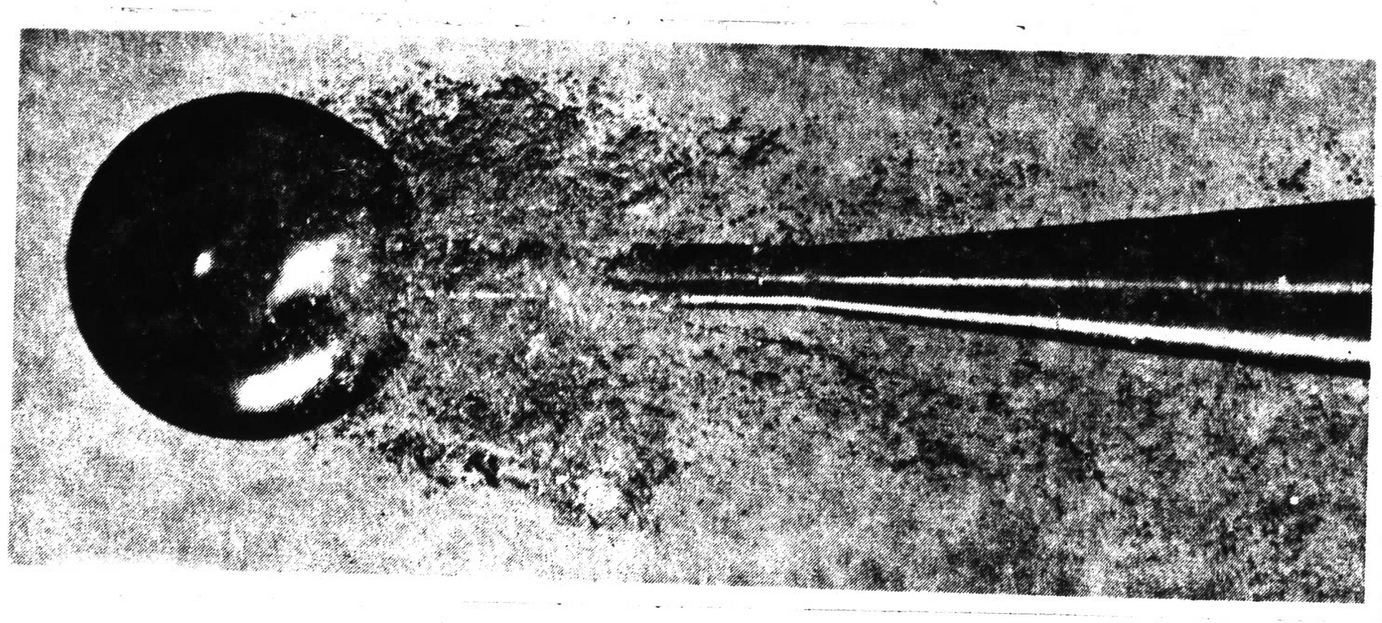

Figure 34. Vortex cavitation at the surface of flow separation behind a sphere [7].

the cavity even if the liquid mass travels into a higher pressure zone. Here however, we encounter a major problem as stated by Knapp: "there has been very little study of the vortex-type cavities and the mechanics involved..." In fact there has been virtually none, primarily due to the complicated nature of the phenomenon. Hours of research reveal that very little work has been done and no convincing theory has been advanced on the nature of the wake vortex at high Reynolds numbers; and it is practically impossible to extend what little has been done to the cavitation situation. Kermeen and Parkin [9] have attempted to formulate a relation for predicting inception at the low pressure centers of vortex cores. They assumed that the inner core was in solid-body rotation and that the motion outside the core was irrotational. Thus, their scale effect due to turbulence can be written

$$P_{r_c} - P_v = (K+C_p)\rho \frac{V_\infty^2}{2} - \rho\left(\frac{\omega a}{2}\right)^2 \qquad (7)$$

where P_{r_c} = static pressure at the vortex core

a = diameter of the vortex core

ω = angular velocity of vortex core

C_p = coefficient of local static pressure.

Use of this formulation still requires specific information about the vortex which is unavailable. Therefore, it

is necessary to retreat to basic concepts and assumptions to demonstrate that the vortex mechanism is probably the cause of inception in a superheated flowing liquid.

EXPERIMENTAL INDICATIONS

Liquid Potassium Results

Experimental data received from John Chen [6] yield results for the pressure differential due to superheating conditions experienced in liquid potassium at inception for various flow speeds. Since the system conditions remained constant throughout the experiments, Reynolds number is directly proportional to velocity. These data are plotted in Figures 35 and 36. The results show a tendency for decreased pressure differential $(P_v - P_\infty)$ as Reynolds number increases, with a leveling off effect displayed for low values of Reynolds number. For zero flow the static pressure throughout the flow field is given by the free stream pressure. If inception could occur in such a situation, the local static pressure, P_L, would also be equal to P_∞. As Reynolds number increases the local static pressure in the region of inception (assumed by the author to be near the vortex core) varies markedly from the free stream value. The free stream velocity influences the intensity of the vortex, which in turn influences the velocity and pressure distribution in

Figure 35. Information pertaining to Brookhaven National Laboratory liquid potassium experiment [6].

Fluid: liquid potassium

Free Stream Pressure: 15.3 psia

Fluid Properties @ 1500°F: density, $\rho = 40.5$ lbm/ft^3

shear coefficient of viscosity,

$\mu = 0.30$ lbm/hr-ft

Dimensions: channel characteristic,

$A = 0.05183$ ft

thermocouple characteristic,

$D = 1/16$ in.

Reynolds Number Relationships:

$$Re_A = \frac{\rho V_\infty A}{\mu}$$

$$\therefore V_\infty = Re_A(4.0(10)^{-5}) \quad \text{[ft/sec]}$$

$$Re_D = \frac{\rho V_\infty D}{\mu} = V_\infty(2.53(10)^3)$$

Data from Figure 7:

Re_A	V_∞	Re_D	$P_\infty - P_{r_c}$
$7(10)^3$	0.28 ft/sec	$.7(10)^3$	2.3 psi
$1(10)^4$	0.40	$1(10)^3$	3.4
$2(10)^4$	0.80	$2(10)^3$	5.5
$4(10)^4$	1.60	$4(10)^3$	7.5
$7(10)^4$	2.80	$7(10)^3$	9.1

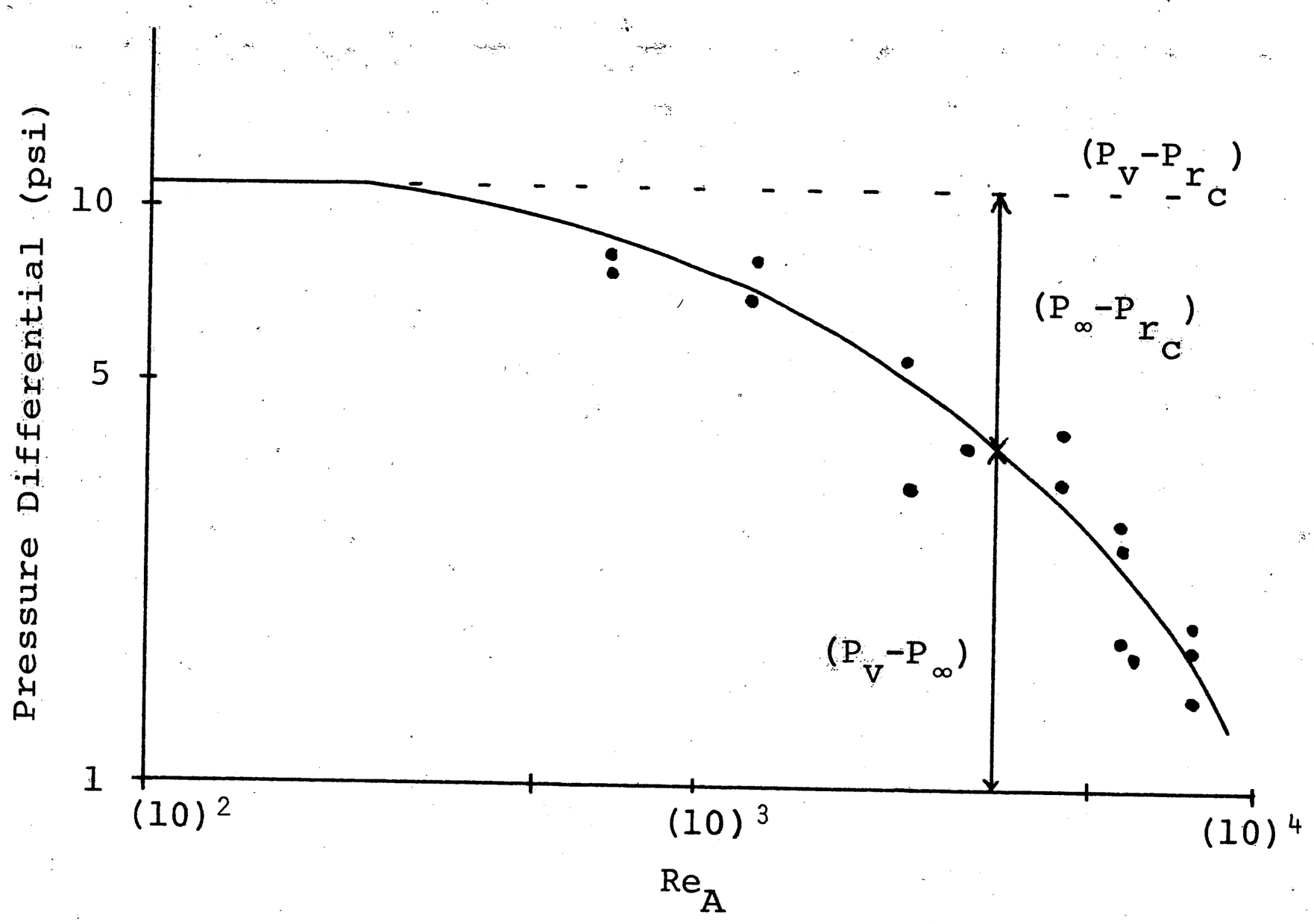

Figure 36. Brookhaven National Laboratory liquid potassium data [6].

the vortex. Therefore, it is not unreasonable to predict that the difference in pressure between the free stream and the vortex core liquid at inception will increase as Reynolds number increases. Realizing this, the author have supposed that the local pressure difference given by $(P_v - P_{r_c})$ remains constant regardless of Re_D. This data will be used in analysis of the vortex core and the pressure potential associated with it. But first it is necessary to show that this supposition does not oppose experimental results which indicate a decrease in superheat as Reynolds number increases.

Explanation of Constant Pressure Differential

The assumption that the local pressure differential remains constant is not so arbitrary as it may appear. As free stream velocity increases, so does the intensity of the vortices shed by a bluff body. Thus, the local pressure in the core tends to decrease with increasing Reynolds number. If the local pressure difference $(P_v - P_{r_c})$ is constant, the vapor pressure must also decrease as Reynolds number increases. Making use of Figure 37, we can see that a decrease in vapor pressure for a constant free stream pressure yields a decrease in the superheat which is achieved in the system. Therefore, the concept of a constant local pressure differential at the inception site predicts that superheat will tend to

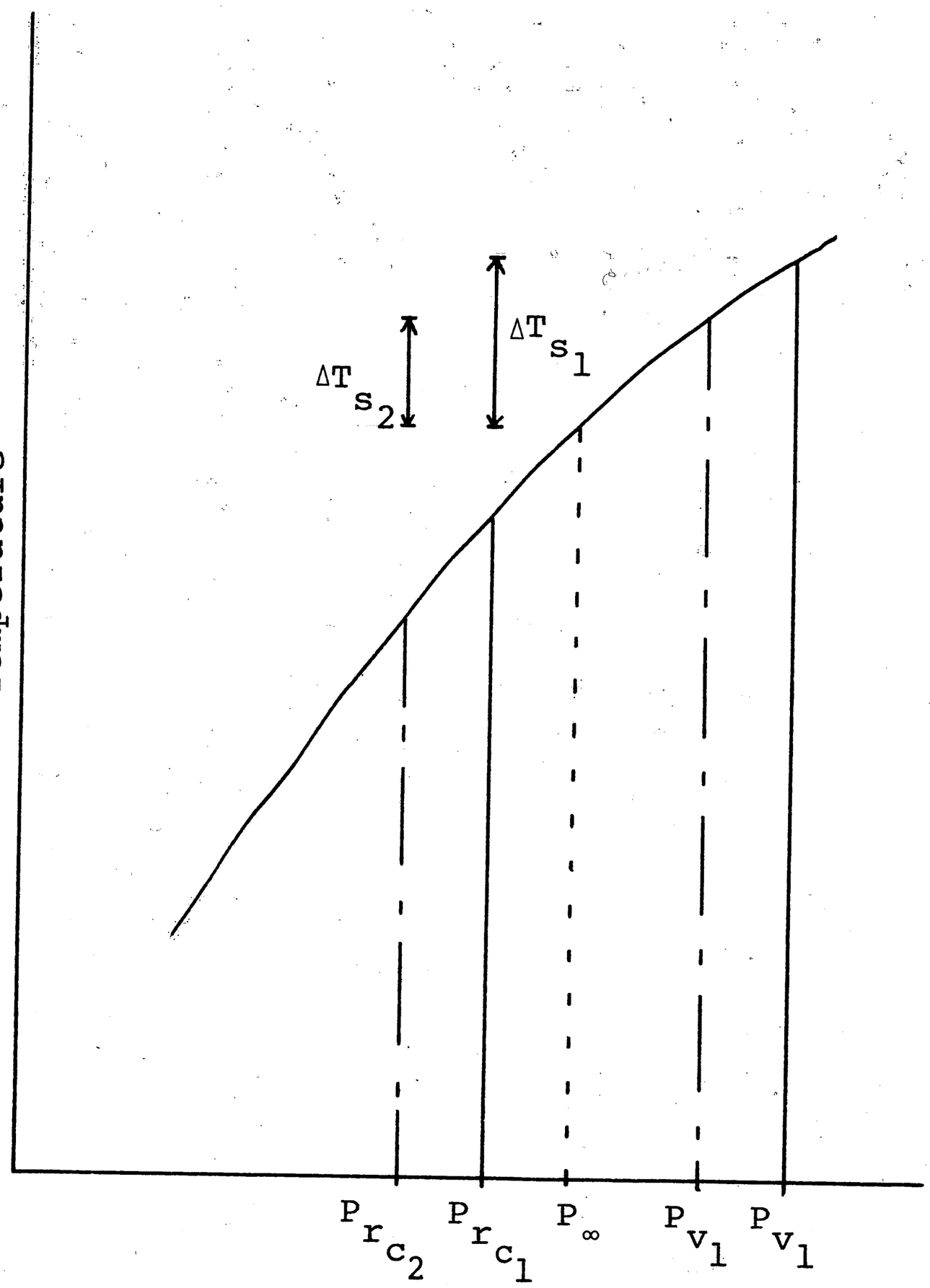

Figure 37. Explanation of decreased superheat for decreased local pressure in the vortex core with pressure differential ($P_v - P_{r_c}$) constant.

decrease as Reynolds number increases. Thus it actually supports previously reported experimental results.

MODELING INCEPTION

Free Vortex Approximation

Consider the flow induced in a stationary fluid by a two-dimensional vortex. $V_r = 0$ and V_θ is only a function of radial position. The continuity equation for the case of plane flow studied in a circular cylindrical coordinate system is

$$\frac{1}{r}\frac{\partial}{\partial r}(rV_r) + \frac{1}{r}\frac{\partial V_\theta}{\partial \theta} = 0. \qquad (8)$$

The stream function, ψ, for such a flow is defined by

$$\frac{\partial \psi}{\partial r} = -V_\theta \quad \text{and} \quad \frac{\partial \psi}{\partial \theta} = rV_r. \qquad (9)$$

Since $rV_r = 0$, the streamlines are circles. Vorticity, $\bar{\omega}$, is equal to the curl of the velocity, or

$$\bar{\omega} = \nabla \times \bar{V}$$

$$= \left(\frac{\partial V_z}{\partial \theta} - \frac{\partial (rV_\theta)}{\partial z}\right)\bar{u}_r - \left(\frac{\partial V_z}{\partial r} - \frac{\partial V_r}{\partial z}\right)r\bar{u}_\theta + \left(\frac{\partial (rV_\theta)}{\partial r} - \frac{\partial V_r}{\partial \theta}\right)\bar{u}_z. \qquad (10)$$

As the flow is two-dimensional and $V_r = 0$, the irrotationality condition is satisfied when rV_θ is constant. Such an irrotational fluid motion is known as a free

vortex. For simplicity we will approximate the wake vortex as a free vortex. The notation that will be used to develop relationships between pressure, velocity, and vortex size is given in Figure 38.

Application of Bernoulli's Equation

If we assume that the fluid is incompressible and irrotational, Bernoulli's equation may be applied to relate velocity and pressure in the vortex. Neglecting variations in height and realizing that velocity has only one component, V_θ, we can reduce the equation to

$$\frac{V_{\theta_1}^2}{2} + \frac{P_1}{\rho} = \frac{V_{\theta_2}^2}{2} + \frac{P_2}{\rho}. \qquad (11)$$

Remembering that the irrotationality condition prescribes that $rV_\theta = C$, a constant, we may write equation (11) as

$$\frac{C^2}{r^2} + \frac{P_r}{\rho} = \frac{C^2}{r^2} + \frac{P_2}{\rho} \qquad (12)$$

or

$$(P_2 - P_r) = \frac{1}{2}\rho C^2\left(\frac{1}{r^2} - \frac{1}{r_2^2}\right). \qquad (13)$$

If position 2 is the exterior of the free vortex, $P_2 = P_{r_v}$ and $r_2 = r_v$. P_r and r are variable with P_r being the pressure at radius r. For most of the vortex region of interest $r << r_v$; therefore, equation (13) becomes

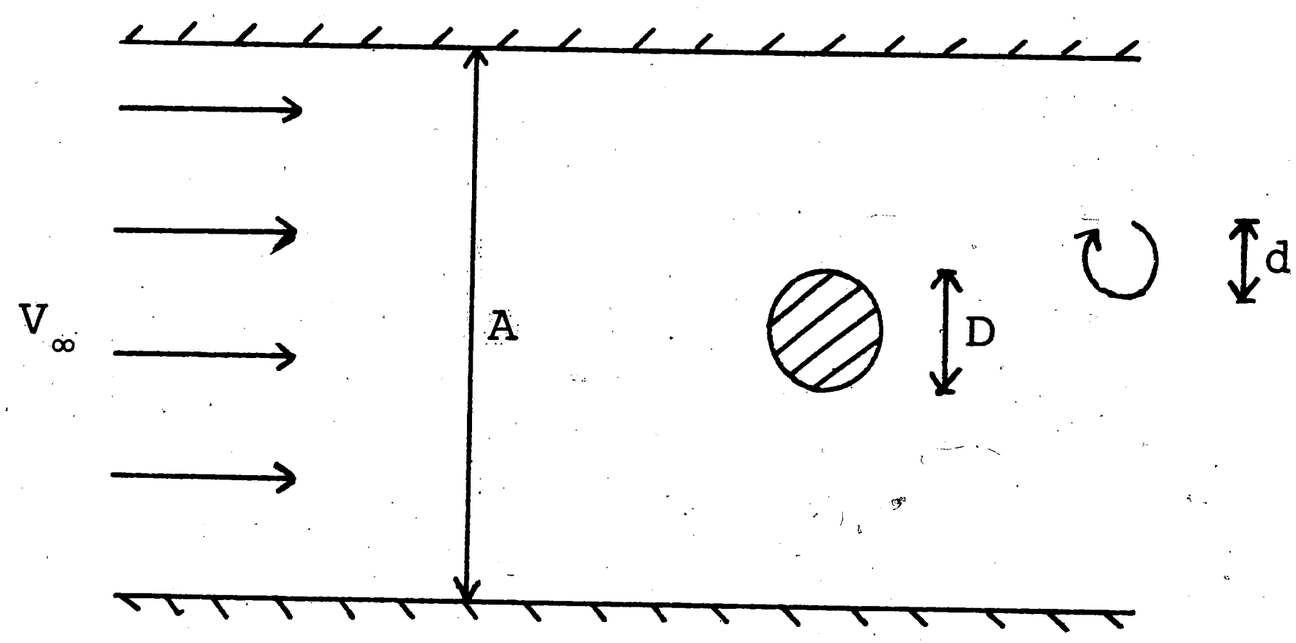

(a) channel detail

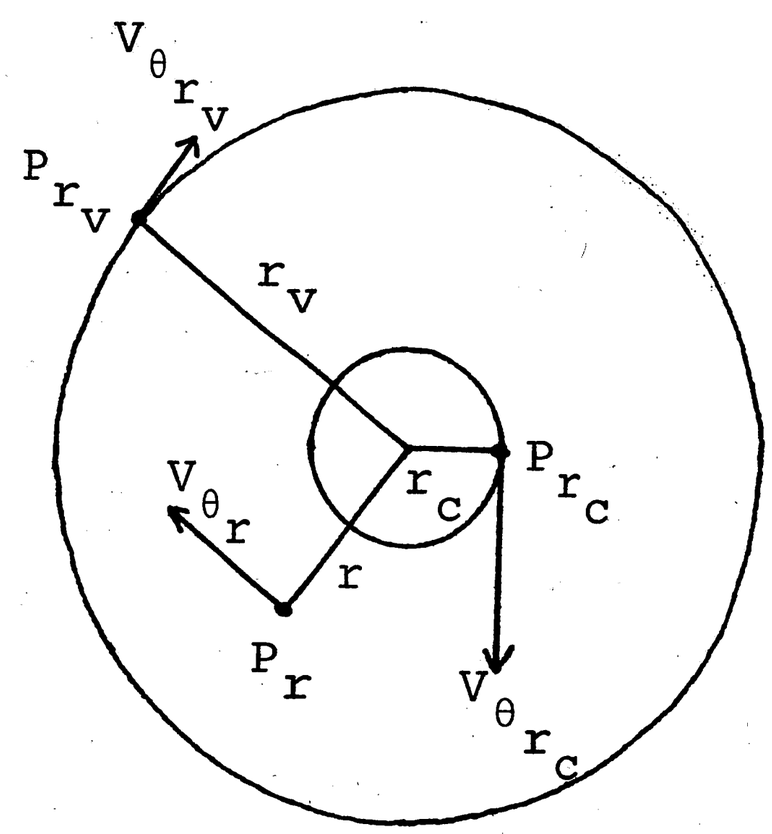

(b) vortex detail

Figure 38. Notation used in describing vortex relationships.

$$(P_{r_v} - P_r) \simeq \frac{1}{2} \rho C^2 \left(\frac{1}{r^2}\right). \qquad (14)$$

Exterior Vortex Pressure

It is of value to us to relate the pressure at the vortex exterior to that of the free stream. For the range of Reynolds numbers reported the pressure coefficient based on surface pressure is experimentally found to be approximately equal to minus one. Using the definition of the pressure coefficient and information from Figure 35, the static pressure in the wake behind the cylinder can be calculated. These results are indicated in Figure 39. In the experimental situation of interest velocities were so low that there is no significant difference between free stream pressure and pressure at the back surface of the cylinder. For this reason it is assumed that the pressure at the exterior of the vortex is equal to that of the free stream. In this light equation (14) may be written as

$$(P_\infty - P_r) \simeq \frac{1}{2} \rho C^2 \left(\frac{1}{r^2}\right). \qquad (15)$$

Critical Radius

For the purpose of discussion it is also of interest to calculate the critical radius necessary for inception to occur. We assume that this value may be found from equilibrium theory:

Figure 39. Calculation of base pressure using definition of pressure coefficient.

$$\text{Coefficient of Pressure, } C_p = \frac{P - P_\infty}{\frac{1}{2}\rho V_\infty^2}$$

$C_p = -1$

$P_\infty = 15.3$ psia

$\rho = 40.5$ lbm/ft^3

$$P = P_\infty - \frac{1}{2}\rho V_\infty^2 = 15.3 - 0.00437\ (V_\infty)^2 \quad \text{[psia]}$$

Re_D	V_∞	P
$.7(10)^3$	0.28 ft/sec	15.3 psi
$1(10)^3$	0.40	15.3
$2(10)^3$	0.80	15.3
$4(10)^3$	1.60	15.3
$7(10)^3$	2.80	15.3

$$r_N = \frac{2\sigma}{P_v - P_{r_c}}. \qquad (16)$$

For liquid potassium at 1500°F the value of surface tension is $0.425(10)^{-2}$ lbf/ft. Zero flow data from Figure 36 indicates that $(P_v - P_{r_c})$ is equal to 11 psi. Therefore, the core radius must be greater than $0.64(10)^{-4}$ inch for nucleation to cccur. For simplicity we will approximate r_N as $(10)^{-4}$ inch.

Reducing Bernoulli's Equation

The pressure differential term on the left in equation (15) may be graphed as a function of radius to yield a series of curves, each representative of a particular value of $C = rV_\theta$. To find values of C representative of the experimental situation of interest we must make an additional assumption.

It seems reasonable to assume that the quantity $\rho V_\theta r/\mu$ would be of the same order of magnitude as the Reynolds number based on the cylinder diameter, Re_D. Equating the two quantities and substituting the definition of C yields

$$C \simeq V_\infty D. \qquad (17)$$

It should be realized that equation (17) is only an approximation, but it indicates that rV_θ is of the order magnitude of $V_\infty D$.

For given values of V_∞, C may be calculated from equation (17). Table 2 includes calculated results for C and C^2 for Reynolds numbers and free stream velocities considered earlier. If C is known, the pressure differential across the vortex may be determined from equation (15) for various values of radii. For these calculations we will assume that a solid core exists in the central region of the vortex with a radius equal to ten times the critical radius necessary for nucleation. Thus we are concerned with radii greater than $(10)^{-3}$ inch.

Results are presented in Table 3 and Figure 40. It is quickly perceivable that large pressure differentials may exist across vortices. A zone of low pressure, therefore, exists for the life of the vortex--a long time relative to the existence of extraneous pressure fluctuations caused by turbulence. Thus, it is reasonable to say that the phenomenon of cavitation is likely to be precipitated by the shedding of high intensity vortices from any protuberance in the system such as a pressure tap or a thermocouple lead.

SUMMARY OF PART II

In summary let us review what has been done. First, it has been realized that in a flowing system the

Table 2. Determination of Constant $C = rV_\theta$

Re_D	V_∞	C	C^2
$.7(10)^3$	0.28 ft/sec	0.00146 ft^2/sec	$2.13(10)^{-6} ft^4/sec^2$
$1(10)^3$	0.40	0.00208	4.33
$2(10)^3$	0.80	0.00416	17.6
$4(10)^3$	1.60	0.00832	69.2
$7(10)^3$	2.80	0.01456	212

Table 3. Determination of Pressure Difference as a Function of Radius for Particular Values of C

(a) $C = 1.46(10)^{-3}$ ft^2/sec

$$P_\infty - P_r = 0.63 \frac{C^2}{r^2} = \frac{1.34(10)^{-6}}{r^2} \quad \text{[psi]}$$

r	$P_\infty - P_r$
$1(10)^{-3}$ in.	1.34 psi
$5(10)^{-3}$	0.0536
$1(10)^{-2}$	0.0134
$5(10)^{-2}$	0.000536

(b) $C = 2.08(10)^{-3}$ ft^2/sec

$$P_\infty - P_r = 0.63 \frac{C^2}{r^2} = \frac{2.73(10)^{-6}}{r^2} \quad \text{[psi]}$$

r	$P_\infty - P_r$
$1(10)^{-3}$ in.	2.73 psi
$5(10)^{-3}$	0.109
$1(10)^{-2}$	0.0273
$5(10)^{-2}$	0.00109

Table 3--continued

(c) $C = 4.16(10)^{-3}$ ft^2/sec

$$P_\infty - P_r = 0.63 \frac{C^2}{r^2} = \frac{10.9(10)^{-6}}{r^2} \qquad \text{[psi]}$$

r	$P_\infty - P_r$
$1(10)^{-3}$ in.	10.9 psi
$5(10)^{-3}$	0.436
$1(10)^{-2}$	0.109
$5(10)^{-2}$	0.00436

(d) $C = 8.32(10)^{-3}$ ft^2/sec

$$P_\infty - P_r = 0.63 \frac{C^2}{r^2} = \frac{43.5(10)^{-6}}{r^2} \qquad \text{[psi]}$$

r	$P_\infty - P_r$
$1(10)^{-3}$ in.	43.5 psi
$5(10)^{-3}$	1.74
$1(10)^{-2}$	0.435
$5(10)^{-2}$	0.0174

Table 3--continued

(e) $C = 14.56(10)^{-3}$ ft^2/sec

$$P_\infty - P_r = 0.63 \frac{C^2}{r^2} = \frac{134(10)^{-6}}{r^2} \quad \text{[psi]}$$

r	$P_\infty - P_r$
$1(10)^{-3}$ in.	134 psi
$5(10)^{-3}$	5.37
$1(10)^{-2}$	1.34
$5(10)^{-2}$	0.0537

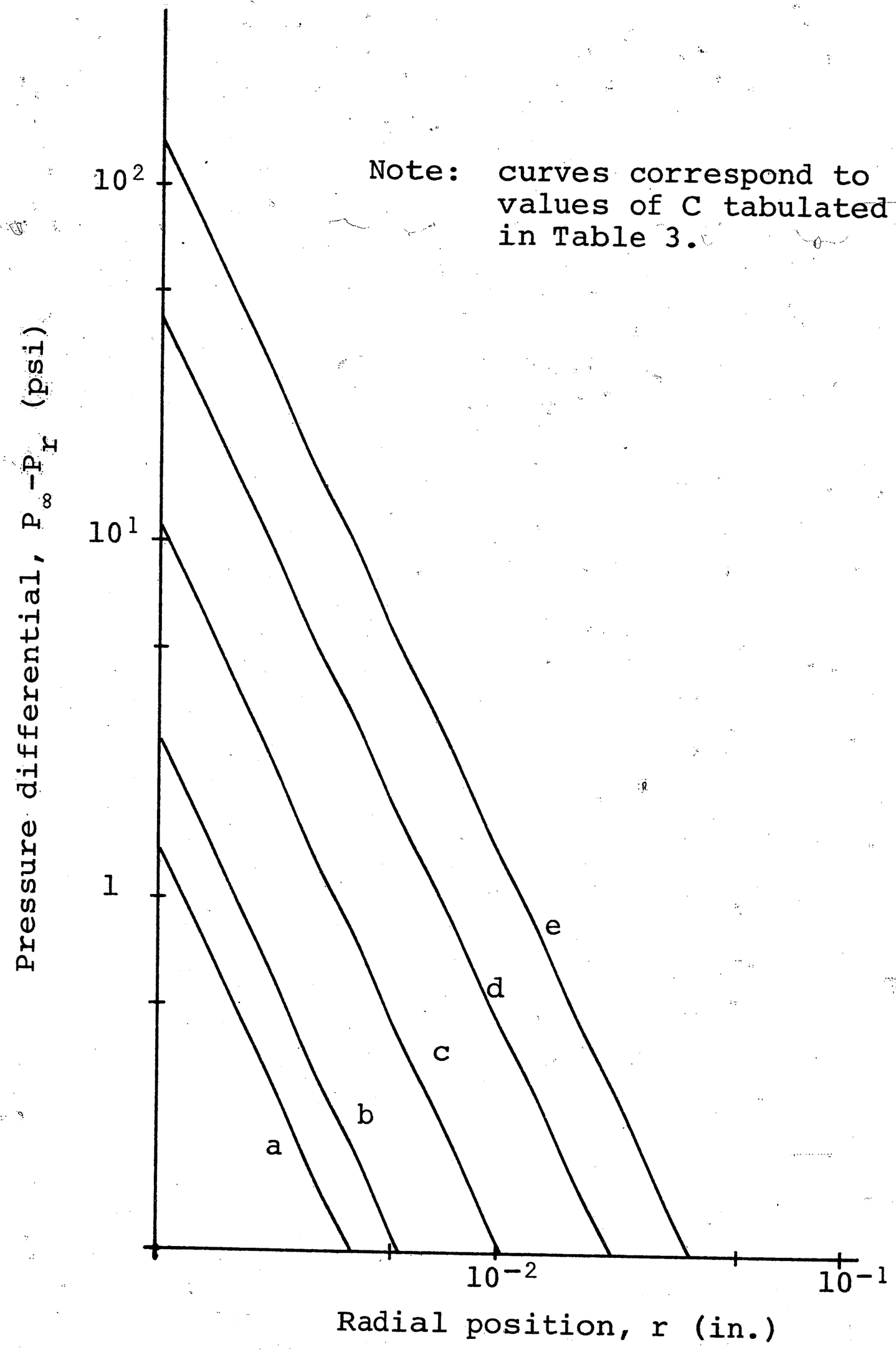

Figure 40. Pressure differential as a function of radial position in a free vortex.

cause of voiding is strongly connected to the phenomenon of cavitation. The pressure mechanism of cavitation as well as the scale effects of critical pressure and vorticity have been described in detail. Also, problems which prevent the application of general parameters and results to the predicting of cavitation in superheated liquids have been mentioned.

To better understand where inception is likely to occur in a flowing system, we have studied the wake characteristics of flow over a bluff body. In particular, the nature of the shed vortex seems to be ideal for inducing inception, since the vortex core is a long-lasting region of high velocity and low pressure relative to the free stream conditions. However, there is a noticeable lack of research and theory concerning the nature of the vortex at high Reynolds numbers.

For this reason an incompressible free vortex is used as a model for an inception site. Since the flow in the vortex model is incompressible and irrotational, Bernoulli's equation may be used to relate pressure and velocity in the region of interest. Data from Brookhaven National Laboratory tests involving liquid potassium indicate a constant local pressure differential at the point of inception and demonstrate that superheat

decreases as Reynolds number increases, as would be predicted by the vortex model. In addition, Bernoulli's equation is further reduced to demonstrate that a large pressure variation is found across the vortex. Realizing that such a variation is very conducive to inception, the author states that inception does occur in the cores of vortices formed by flow around and over irregularities in the system.

The author had hoped to be able to produce work of a more substantive nature in this study, and it must be noted that none of the material is highly conclusive. Instead, it is theory which must wait to be tested until more research on the nature of high speed vortices has been completed.

TERMINOLOGY - PART II

English Letter Notation

A	test section diameter
a	vortex core diameter
C	constant
C_p	coefficient of local static pressure
D	bluff body diameter
d	vortex exterior diameter
K	cavitation number
P	static pressure
P_b	bubble pressure
P_L	local liquid pressure
P_r	pressure at radius r
P_{r_c}	pressure at vortex core
P_{r_v}	pressure at vortex exterior
P_v	vapor pressure
P_∞	free stream pressure
R	bubble radius
r	radial position
r_c	vortex core radius
r_N	critical radius for nucleation
r_v	vortex exterior radius
Re_A	Reynolds number based on test section diameter
Re_D	Reynolds number based on bluff body diameter
T	temperature

T_∞	free stream temperature
t	time
V_r	radial velocity
V_θ	angular velocity
V_z	vertical velocity
V_∞	free stream velocity
V_{θ_r}	velocity at radius r
$V_{\theta_{r_c}}$	velocity at vortex core
$V_{\theta_{r_v}}$	velocity at vortex exterior
z	vertical position

Greek Letter Notation

β	velocity function
θ	angular position
μ	shear coefficient of viscosity
ρ	liquid density
σ	surface tension
ψ	stream function
ω	vorticity

Vector Notation

$\bar{v}$	velocity
$\bar{u}_r$	unit vector in radial direction
$\bar{u}_\theta$	unit vector in angular direction
$\bar{u}_z$	unit vector in vertical direction
$\bar{\omega}$	vorticity

BIBLIOGRAPHY

1. Murphy, R. W., and Bergles, A. E., "Subcooled Flow Boiling of Fluorocarbons--Hysteresis and Dissolved Gas Effects on Heat Transfer," to be presented at 1972 Heat Transfer and Fluid Mechanics Institute.

2. Mood, A. M., Introduction to the Theory of Statistics, New York: McGraw-Hill, 1950.

3. Haugen, E. B., Probabilistic Approaches to Design, New York: John Wiley, 1968.

4. Poritsky, H., "The Collapse or Growth of a Spherical Bubble or Cavity in a Viscous Fluid," Proc. First U.S. Natl. Congr. Appl. Mech. (ASME), (1952), pp. 813-21.

5. Kermeen, R. W., and Parkin, B. R., "Incipient Cavitation and Wake Flow behind Sharp-edged Disks," Calif. Inst. of Tech. Engr. Div. Rep. 85-4, 1957.

6. Lehigh University, Bethlehem, Pa. Personal conversations with John C. Chen, Professor of Mechanical Engineering, 1972.

7. Birkhoff, G., and Zarantonello, E. H., Jets, Wakes, and Cavities, New York: Academic Press, 1957.

8. Hoffman, H. W., and Cox, B., "A Preliminary Collation of the Thermodynamic and Transport properties of Potassium," Contract No. W-7405-eng-26, Oak Ridge National Laboratory, 1968.

9. Kermeen, R. W., Parkin, B. R., and McGraw, J. T., "Mechanism of Cavitation Inception and the Related Scale-effects Problem," Trans. ASME, Vol. 77 (1955), pp. 534-541.

10. Knapp, R. T., Daily, J. W., and Hammitt, F. G., Cavitation, New York, McGraw-Hill, 1970.

11. Owczarek, J. A., Introduction to Fluid Mechanics, Scranton: International Textbook, 1968.

APPENDIX

General Procedures for Conducting Inception Tests for Constant Superheats

1. Attach supply siphon and add 55 ml of clean Freon 113 to the test tube.
2. Immerse the specimen in 500 ml of water at 70°F so that 50 ml of Freon are below the bath surface level. Let sit for 15 minutes after agitating for 15 seconds.
3. Fill the heated bath with 950 ml of water and turn on heaters to proper settings for desired test.
4. Turn the stirrer variac control to 170, then back to 160 to maintain proper bath circulation.
5. Stabilize the condenser flow and temperature, and check the system tubing and collection bottle.
6. After bath is at desired temperature and specimen has been in pre-bath for 15 minutes, transfer tube to heated bath and begin test.
7. At inception remove the specimen from the test tube and continue procedure beginning with step 1 again.

General Procedure for Conducting Inception Tests for Constant Temperature Ramps

1. Attach supply siphon and add 55 ml of clean Freon 113 to the tube.
2. Fill the heated bath with 950 ml of water at 70°F and immerse the specimen so that 50 ml of Freon are below

the bath surface level. Let sit for 15 minutes after agitating for 15 seconds.

3. Stabilize the condenser flow and temperature, and check the system tubing and collection bottle.
4. After specimen has been in bath at 70°F for 15 minutes, turn on heaters to proper settings for desired test.
5. Turn the stirrer variac control to 170, then back to 160 to maintain proper bath circulation.
6. Adjust heaters as necessary to maintain a constant temperature ramp during the test.
7. At inception remove the specimen from the test tube and continue procedure beginning with step 1 again.

VITA

John J. Morgan, born in Upper Darby, Pennsylvania on May 18, 1949, the son of William and Eleanor Morgan, attended Lehigh University as an undergraduate student in the College of Engineering. He received the degree of Bachelor of Science in Mechanical Engineering on June 13, 1971, graduating with highest honors. Continuing his studies at Lehigh, he completed the requirements for the degree of Master of Science in Mechanical Engineering--excepting the final drafting of this thesis--in August, 1972 and is now employed as a machinery development engineer at DuPont's Engineering Development Laboratory in Wilmington, Delaware.